the plant journal

SEB SOCIETY FOR EXPERIMENTAL BIOLOGY

The Plant Journal (2023) doi: 10.1111/tpj.16104

Fine mapping of meiotic crossovers in *Brassica oleracea* reveals patterns and variations depending on direction and combination of crosses

Chengcheng Cai[1,2], Alexandre Pelé[3], Johan Bucher[1], Richard Finkers[1,4] and Guusje Bonnema[1,2,*]

[1]*Plant Breeding, Wageningen University and Research, 6708 PB, Wageningen, The Netherlands,*

[2]*Graduate School Experimental Plant Sciences, Wageningen University and Research, 6708 PB, Wageningen, The Netherlands,*

[3]*Laboratory of Genome Biology, Institute of Molecular Biology and Biotechnology, Adam Mickiewicz University in Poznan, 61-614, Poznan, Poland, and*

[4]*Gennovation B.V., Agro Business Park 10, 6708 PW, Wageningen, The Netherlands*

Received 12 July 2022; revised 3 January 2023; accepted 5 January 2023.

*For correspondence (e-mail guusje.bonnema@wur.nl).

SUMMARY

Meiotic recombination is crucial for assuring proper segregation of parental chromosomes and generation of novel allelic combinations. As this process is tightly regulated, identifying factors influencing rate, and distribution of meiotic crossovers (COs) is of major importance, notably for plant breeding programs. However, high-resolution recombination maps are sparse in most crops including the *Brassica* genus and knowledge about intraspecific variation and sex differences is lacking. Here, we report fine-scale resolution recombination landscapes for 10 female and 10 male crosses in *Brassica oleracea*, by analyzing progenies of five large four-way-cross populations from two reciprocally crossed F1s per population. Parents are highly diverse inbred lines representing major crops, including broccoli, cauliflower, cabbage, kohlrabi, and kale. We produced approximately 4.56T Illumina data from 1248 progenies and identified 15 353 CO across the 10 reciprocal crosses, 51.13% of which being mapped to <10 kb. We revealed fairly similar Mb-scale recombination landscapes among all cross combinations and between the sexes, and provided evidence that these landscapes are largely independent of sequence divergence. We evidenced strong influence of gene density and large structural variations on CO formation in *B. oleracea*. Moreover, we found extensive variations in CO number depending on the direction and combination of the initial parents crossed with, for the first time, a striking interdependency between these factors. These data improve our current knowledge on meiotic recombination and are important for *Brassica* breeders.

Keywords: *Brassica oleracea*, crossover, gene density, genetic background, meiotic recombination, sex difference, structural variation.

INTRODUCTION

Meiotic recombination is crucial in a plant's life cycle as it assures proper segregation of parental chromosomes during meiosis, thus guaranteeing genome integrity and stability. In addition, meiotic recombination is a key driving force for creating novel allelic combinations, enabling plant breeders to combine desired alleles and eliminate deleterious mutations (Li et al., 2015; Martin & Wagner, 2009; Wijnker & de Jong, 2008). Meiotic recombination is initiated in prophase I of meiosis by the formation of many DNA double-strand breaks (DSBs; Mercier et al., 2015). However, this process is tightly controlled and only a small fraction of DSBs results in reciprocal exchanges between homologous non-sister chromatids, also referred to as crossovers (COs; De Muyt et al., 2009; Mercier et al., 2015), due to anti-CO factors (Crismani et al., 2012; Mieulet et al., 2018; Séguéla-Arnaud et al., 2015). Moreover, besides the mandatory CO formed per chromosome pair, which ensures their proper segregation, rarely more are observed due to the so-called phenomenon of CO interference that reduces the chance of two close-by COs (Mercier et al., 2015; Muller, 1916; Sturtevant, 1915). In most species, two types of meiotic COs coexist (De Muyt et al., 2009). Class I COs, contributing about 85%, notably rely on the ZMM complex, and are subject to CO interference, whereas Class II COs, representing

15% of all COs, are unaffected by CO interference and rely on *MUS81* protein (Mercier et al., 2015; Mezard et al., 2007; Osman et al., 2011).

COs are not uniformly distributed along the chromosomes in almost all studied species (Kianian et al., 2018; Mézard et al., 2015). Typically, they are concentrated in distal regions and always suppressed in centromeric and pericentromeric regions (Dreissig et al., 2019; Marand et al., 2017; Raz et al., 2021). In plants, recombination landscapes with high CO resolution have been established in the model species *Arabidopsis* and a very limited number of crops with generally more complex genomes, such as maize (Kianian et al., 2018) and potato (Marand et al., 2017), allowing investigation of the influence of associated genomic and epigenomic features. This is however lacking in many other genera such as *Brassica*, with CO maps of *Brassica rapa* (Pelé et al., 2017) and *Brassica napus* (Boideau et al., 2022) generated with limited numbers of single nucleotide polymorphism (SNP) markers. It has been found that the occurrence of COs positively correlates with gene density that is generally high in distal regions and negatively with transposable element (TE) density, which is highest at and next to centromeres (Anderson et al., 2006; Dooner & He, 2008; Erayman et al., 2004; Wu et al., 2003). Sequence divergence is another important genomic factor with a complex relationship with meiotic recombination, which varies across different scales and chromosomal contexts (Blackwell et al., 2020; Serra et al., 2018). Small-scale sequence divergence, such as SNPs and small InDels, are associated with increased recombination frequency (Lian, Solier, Walkemeier, Huettel, et al., 2022; Ziolkowski et al., 2015). In natural populations of multiple species, positive correlations were observed between SNP density and the historical CO landscape, which is measured from linkage disequilibrium (LD; Begun & Aquadro, 1992; Cutter & Payseur, 2013; Gore et al., 2009; Nordborg et al., 2005; Paape et al., 2012; Spencer et al., 2006). In Arabidopsis, juxtaposition of heterozygous and homozygous regions results in increased recombination frequency in heterozygous regions while decreased recombination frequency is shown in homozygous regions (Blackwell et al., 2020; Ziolkowski et al., 2015). Blackwell et al. (2020) discovered a parabolic relationship between SNP density and recombination frequency, with initially a positive relationship and then a negative relationship along with the increase of SNP density. In tomato, Fuentes et al. (2022) found a significant positive overlap between short deletions (<500 bp) and recombination hotspots, suggesting that small InDels do not suppress recombination. However, large-scale structural rearrangements have suppressive effects on recombination (Boideau et al., 2022; Lian, Solier, Walkemeier, Huettel, et al., 2022; Rowan et al., 2019). In Arabidopsis, the approximately 1.2-Mb inversion between Col and L*er* on chromosome 4 inhibits recombination in this region (Lian, Solier, Walkemeier, Huettel, et al., 2022; Rowan et al., 2019). A 70-kb transposition on chromosome 3 identified between *Arabidopsis thaliana* accessions BG-5 and Kro-0 also displayed extreme local suppression of recombination (Alhajturki et al., 2018; Rowan et al., 2019). In *B. napus*, Boideau et al. (2022) discovered large inversions (>1 Mb) in two most distal non-pericentromeric regions lacking recombination, suggesting that Mb-scale inversions prevent recombination. The causality for the strong correlation between sequence divergence and CO occurrence is still poorly understood. In a recent study, Lian, Solier, Walkemeier, Huettel, et al. (2022) hypothesized that polymorphisms are not causal for the shape of the Mb-scale recombination landscape in Arabidopsis but, on the contrary, recombination contributes to shaping the sequence divergence across the genome. Besides genomic factors, epigenetic features, such as DNA methylation, histone modifications, and nucleosome occupancy, also locally affect CO formation (Choi et al., 2013, 2018; Habu et al., 2015; Melamed-Bessudo & Levy, 2012; Mirouze et al., 2012; Yelina et al., 2012).

Despite the strong regulation of CO number and distribution, extensive variation is observed both between and within species. Factors responsible for these variations have the potential to profoundly influence selective responses and facilitate adaptation (Coop & Przeworski, 2007; Feldman et al., 1996; Nei, 1967), all the while being of interest for plant breeders (Wijnker & de Jong, 2008). On the one hand, a large range of external factors such as temperature fluctuation, nutritional status, or pathogen attack result in CO variations (Dreissig et al., 2019; Henderson & Bomblies, 2021; Modliszewski & Copenhaver, 2017). On the other hand, intraspecific differences in CO rates are observed in the same environment. This is well illustrated in *A. thaliana* for which CO rates vary twofold among dozens of accessions tested in selected intervals (Ziolkowski et al., 2015). In crops, similar observations were repeatedly made, as exemplified in maize from which the study of 23 doubled-haploid populations revealed intraspecific variation of recombination rates and landscapes (Bauer et al., 2013). Marked differences in CO level and pattern were also observed between male and female meiosis; a phenomenon referred to as heterochiasmy (Capilla-Pérez et al., 2021; Lenormand, 2003; Lenormand & Dutheil, 2005; Sardell & Kirkpatrick, 2020). In Arabidopsis Col-0 × L*er* populations, many more COs were observed in male than female meiosis (Drouaud et al., 2007; Giraut et al., 2011; Lian, Solier, Walkemeier, Huettel, et al., 2022). Moreover, the Mb-scale recombination landscapes were remarkably different with distal regions displaying the highest recombination rates in male meiocytes and the lowest in female meiocytes (Lian, Solier, Walkemeier, Durand, et al., 2022). However, this is not a universal feature of plants. Indeed,

some species such as *B. oleracea* showed a reverse pattern with more COs formed in female meiosis (Kearsey et al., 1996), and others such *B. napus* or *Coffea canephora* exhibiting similar CO levels in male and female meiosis, thus no heterochiasmy (Kelly et al., 1997; Lashermes et al., 2001; Lenormand & Dutheil, 2005). Interestingly, in maize no differences between male and female CO levels were observed in the B73 × Mo17 background, while the Zheng58 × SK background revealed heterochiasmy with more COs generated during male meiosis (Kianian et al., 2018; Luo et al., 2019). This latter observation suggests that heterochiasmy could be dependent on the genetic background; however, studies to support this suggestion, focusing on interaction of both factors on meiotic recombination, remain sparse.

In this study, we investigated recombination variation among 10 different genetic backgrounds (hereafter also referred to as crosses/cross combinations) in *B. oleracea*, a diploid species displaying enormous phenotypic variation between different morphotypes, and studied the sex differences for each cross. To do so, we constructed five large four-way-cross (FwC) populations with each two F1s being reciprocally crossed per population. In total, we sequenced 1248 progeny genomes and harvested approximately 4.56T Illumina data for the five FwC populations. From this fine mapping, we identified a total of 15 353 COs and characterized recombination landscapes for all 10 female and male crosses. We revealed key genomic factors that shape the recombination landscape in *B. oleracea*, with gene density and large-scale structural variations (SVs) influencing genome-wide and local CO formation, respectively. While Mb-scale recombination landscapes were fairly similar among the 10 sex-averaged as well as female-/male-specific crosses, we highlight extensive variations in CO number among different crosses and heterochiasmy in some cross combinations, revealing that CO variation in *B. oleracea* is shaped by genetic background, heterochiasmy and their interaction.

RESULTS

CO identification

We previously generated five chromosome-scale genome assemblies of five homozygous *B. oleracea* morphotypes, including broccoli, cauliflower, kale, kohlrabi, and white cabbage (Cai et al., 2022). To explore the recombination landscapes in *B. oleracea*, we constructed five FwC populations using the above five genotypes as founders, each including four different parents representing four different morphotypes (Figure S1; Figure 1). For each FwC population, the two F1s were reciprocally crossed to analyze independently female and male meiosis (Figure 1). The five FwC populations included a total of 1248 progenies (Figure 1) for which we obtained approximately 4.56T data through Illumina paired-end genome sequencing, with an average of 6.55-fold coverage per progeny (Table S1). By mapping reads to the broccoli reference genome that is one of the five parents, we called SNPs for the parental genomes and progenies. We selected 184 152–413 849 (0.35–0.79 SNP per kb) segregating SNPs in each of the 10 reciprocal crosses for CO analyses (Table 1), which were distributed uniformly and genome-wide across the nine chromosomes (Figure S2).

Each set of SNPs was independently subjected to phaseLD for CO identification, which implemented sliding windows, Bayesian inference, and logistic regression approaches (Marand et al., 2017). In total, we identified 15 353 COs from the 10 reciprocal crosses with 7492 and 7861 COs arising during female and male meiosis, respectively (Figure S3; Table 1). This translates into an average of approximately 6.27 and approximately 6.64 COs per female and male gamete, respectively. Over all 10 sex-averaged crosses, we identified 5.80–7.02 COs per haploid gamete over the 2377 (1194 female and 1183 male gametes) analyzed (Figure 5a). The distribution of total CO number (TCN) per gamete across the 10 reciprocal crosses follows a normal distribution (Figure S4). The high SNP marker densities enabled the fine-scale identification of COs, resulting in a median resolution of 9088 bp for the pool of 10 sex-averaged crosses, with 89.16, 80.26, and 51.13% COs having an interval resolution lower than 200, 100, and 10 kb, respectively (Table 1). The observed distributions of CO number for all nine chromosomes in all 10 sex-averaged crosses revealed that most gametes exhibit between 0 and 1 CO per chromatid (Figure S5a). The rare occurrence of multiple COs per chromatid suggests elevated CO interference. On average, 74.10–96.97% of gametes had 0 or 1 CO in each of the nine chromosomes across the 10 sex-averaged crosses, with larger chromosomes (i.e., C3, C4, C5, and C9) displaying more multiple (≥2) COs (Figure S5a). To analyze CO interference in a model-independent way, we calculated the physical distance between adjacent COs only using chromosomes of gametes having at least two COs. In all the 10 cross combinations, distributions of adjacent CO distance clearly peaked about 50–55 Mb. By contrast, the corresponding "non-interference" distributions (see "Experimental procedures" section) mainly peaked at lower values (<5 Mb), validating strong CO interference in *B. oleracea* (Figure S6a). Accordingly, the interference strengths as indicated by Kullback–Leibler (KL) divergence among the 10 sex-averaged crosses were similar (Table S2). Under the hypothesis of random CO placements and independent CO events, CO numbers per chromatid are expected to follow a Poisson distribution. Comparison between the observed CO number distributions and expected Poisson distributions revealed a deficit in gametes with 0 CO and an excess of gametes with 1 CO (Figure S5a,b), fitting the occurrence of an

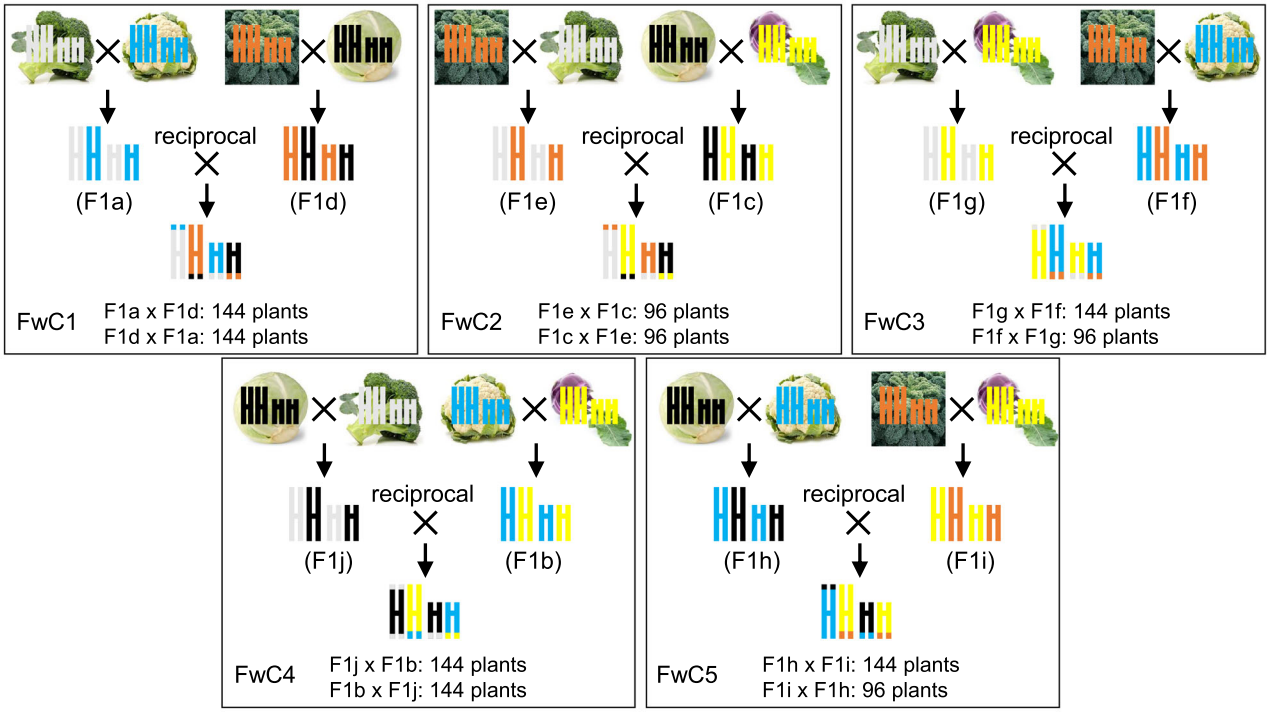

Figure 1. Crossing scheme with five parental essentially homozygous lines, representing five different *Brassica oleracea* morphotypes.
Five morphotypes are pairwise intercrossed to generate 10 F1 hybrids (F1a–F1j). F1s are then intercrossed in both directions to generate four-way-cross (FwC) populations. Meiotic recombinations of all 10 combinations of the five morphotypes can be studied with these five FwC populations. Number of progenies collected for each FwC population is indicated in the figure. *B. oleracea* has nine pairs of chromosomes: here only two sets are depicted. For each FwC population, one progeny is depicted with recombined chromosomes, where colors depict parental origin.

obligate CO that ensures proper segregation of homologous chromosomes.

Pattern of recombination landscape strongly relies on genomic features

To compare recombination landscapes among the 10 sex-averaged crosses on a genome-wide scale, we calculated the CO frequencies using 2-Mb sliding windows with 50 kb steps and plotted this along *B. oleracea* chromosomes. Interestingly, we revealed remarkably similar recombination landscapes among the 10 crosses deriving from different parental combinations of the five *B. oleracea* morphotypes (Figure 2a; Figure S7). The *B. oleracea* genome includes three acrocentric (C6, C7, and C8) and six (sub)metacentric chromosomes (C1–C5 and C9). In all the 10 crosses, the highest CO frequencies were observed in distal regions of both arms in the (sub)metacentric chromosomes, whereas COs were markedly suppressed at centromeric and pericentromeric regions. For the acrocentric chromosomes, besides centromeric and pericentromeric regions, COs were also strongly suppressed in the short arm; however, CO rates were the highest in distal regions of the long arm. We found significant positive correlations between the CO landscapes of different cross combinations, in the range of 0.79–0.87 (Spearman's rank correlation, $P < 0.0001$; Figure 2b). The conserved recombination landscapes under the given window size are independent of the level of polymorphisms and SVs between the two parental genomes.

The 7852 (480–1086 COs in each of the 10 sex-averaged crosses) fine-resolution scale COs with interval length <10 kb were selected to analyze their potential associations with various genomic features. We found that 50.42–57.29% of COs in each of the 10 sex-averaged crosses overlapped with gene bodies (exons and introns) (Figure 3a). Interestingly, more than half of these COs (31.54–39.04% of total COs) overlapped with exons, while exon and intron sequences occupied only 10.92% and 9.03% space in the reference genome (Figure 3c), respectively. In contrast, only 13.28–18.15% of COs overlapped with TEs, which account for more than 53% of the genome. In comparison with random CO sites generated from 10 000 permutations, the observed CO sites were significantly enriched in gene bodies and their flanking 1 kb regions, but significantly depleted in TEs (empirical, $P < 0.0001$) (Figure 3b). Permutation tests performed by regioneR (Gel et al., 2016) also suggested that genes and COs overlap significantly more than expected by chance in all crosses (Figure S8). Together, these results suggest the regional preference of CO sites. More than 99% of fine-

Table 1 Summary of crossovers (COs) identified for the five four-way-cross (FwC) populations

Population	Cross[a]	Number of gamete[b]	CO studied	Female/male	SNPs used for CO identification	Total number of CO	median resolution (bp)	No. of CO with resolution within 200 kb	No. of CO with resolution within 100 kb	No. of CO with resolution within 10 kb
FwC1	F1a × F1d	141	broccoli × cauliflower	Female	263 618	906	4463	859	790	541
		141	kale × white	Male	298 508	881	9684	803	725	445
	F1d × F1a	135	broccoli × cauliflower	Male	247 307	974	6068	892	803	545
		140	kale × white	Female	294283	862	5958	802	724	476
FwC2	F1e × F1c	94	kale × broccoli	Female	274 274	679	8695	618	565	356
		96	white × kohlrabi	Male	184 152	573	30 414	436	380	225
	F1c × F1e	96	kale × broccoli	Male	413 849	644	4675	610	559	385
		95	white × kohlrabi	Female	233 330	608	22 623	481	412	255
FwC3	F1f × F1g	92	kale × cauliflower	Female	409 758	482	10 141	430	375	239
		92	broccoli × kohlrabi	Male	244 283	643	11 379	563	507	311
	F1g × F1f	131	kale × cauliflower	Male	294 161	811	11 203	727	642	386
		131	broccoli × kohlrabi	Female	207 906	922	12 389	823	726	434
FwC4	F1j × F1b	138	white × broccoli	Female	331 205	919	3923	861	795	555
		133	cauliflower × kohlrabi	Male	262 210	890	11 644	790	703	424
	F1b × F1j	135	white × broccoli	Male	278 731	918	8060	820	748	481
		136	cauliflower × kohlrabi	Female	238 850	801	13 896	692	617	363
FwC5	F1i × F1h	92	kale × kohlrabi	Female	292 207	559	10 525	494	439	275
		91	white × cauliflower	Male	352 797	604	8018	529	488	326
	F1h × F1i	133	kale × kohlrabi	Male	231 516	923	15 309	781	702	418
		135	white × cauliflower	Female	317 912	754	7028	677	622	412

CO, crossover; SNP, single nucleotide polymorphism; White, white cabbage.

[a]F1a–F1j correspond to the 10 F1 hybrids as shown in Figure 1.

[b]Number of gametes after removing samples based on the amount of sequencing data and total CO number per gamete (see "Experimental procedures" section).

The Plant Journal, (2023), doi: 10.1111/tpj.16104

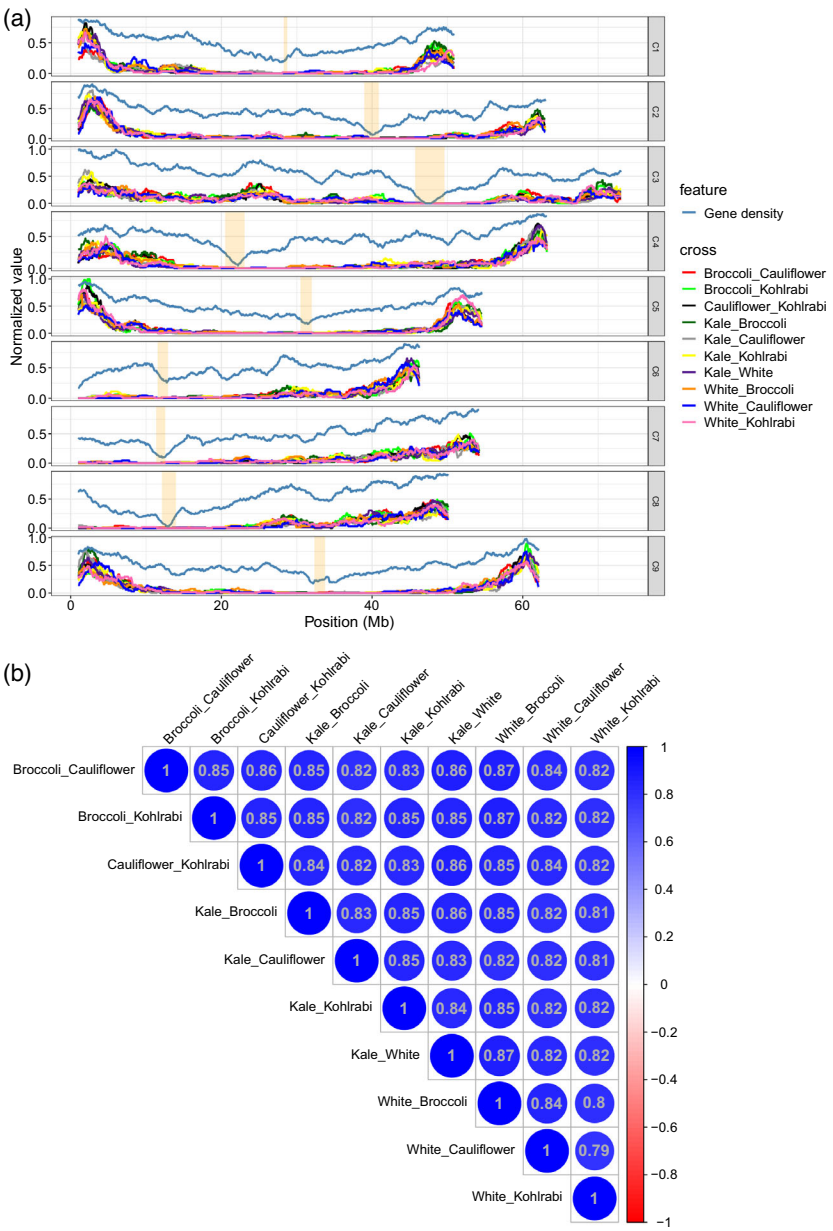

Figure 2. Recombination landscapes for the 10 sex-averaged crosses.
(a) Crossover (CO) rate and gene density distributions along the nine chromosomes of *Brassica oleracea*. Analysis is done with 2-Mb sliding windows and 50-kb step sizes. Centromere regions are indicated by orange shadings. CO rate and gene density values are normalized to 0 to 1. See Figure S6 for the figures of CO rates before normalization.
(b) Genome-wide correlation coefficient (the Spearman's correlation) matrices among the 10 sex-averaged CO distributions.

resolution COs in each of the 10 crosses were located within 10 kb of a gene and the distributions showed a similar pattern among the 10 sex-averaged crosses (Figure 3d). Gene density distribution (2-Mb sliding windows with 50 kb steps) was strongly correlated with the 10 sex-averaged recombination landscapes, with high CO rates in distal gene-rich regions (Figure 2a; Figure S7). More interestingly, we found that "CO bumps" in regions (i.e., C3, C6, and C8) that were far from distal regions in all 10 crosses were also associated with increased gene density compared with that of their nearby regions (Figure 2a).

Recombination frequency strongly correlates with sequence polymorphisms, as observed in natural populations of many species, with historical recombination events positively correlated with SNP densities (Blackwell et al., 2020; Lian, Solier, Walkemeier, Huettel, et al., 2022). The 10 genetic backgrounds in our study showed varying levels of small-scale sequence

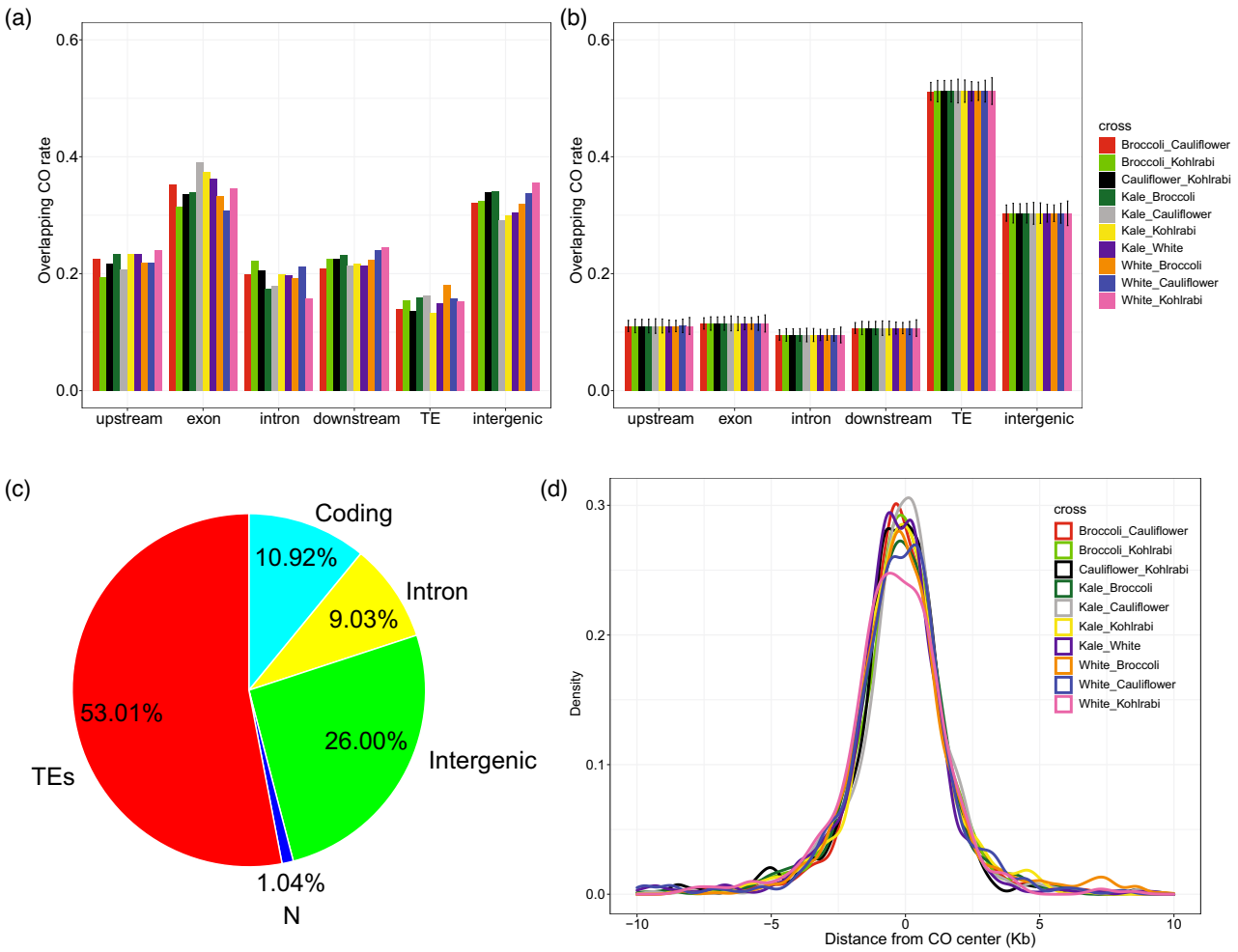

Figure 3. Genomic features associated with crossovers (COs) for the 10 sex-averaged crosses.
(a) Overlap analysis of observed COs with different genomic features.
(b) Overlap analysis of random regions derived from 10 000 simulations with different genomic features, with error bars denoting the standard deviation. (a,b) CO interval was used for the overlap analysis. If an interval overlapped with multiple genomic features, the interval was counted towards each genomic feature.
(c) Percentage of genomic components in the broccoli reference genome. TE, transposable element.
(d) Distribution of distance from each CO to the nearest gene. Middle position of both CO interval and gene was used for calculating the distance.

divergence (Table S3), allowing to explore further the relationship between CO occurrence and polymorphism. The distribution of parental SNPs along chromosomes showed strong local differences among the 10 crosses, particularly near-centromeric regions in several chromosomes (Figure S9). Genome-wide, we observed weak but significant positive correlations between SNP density and CO rate in all the 10 sex-averaged crosses (Spearman's rank correlation, ρ = 0.15–0.30, $P < 0.0001$). Consistent with Arabidopsis (Blackwell et al., 2020), we found a parabolic relationship between SNP density and CO rate, with a high CO rate being associated with moderate SNP density (Figure S10a). Although pericentromeric regions contribute remarkably to this relationship, a weak parabolic relationship can still be observed when excluding these regions (Figure S10b). In our data, we did not find significantly different recombination patterns when comparing regions with the most striking differences in SNP densities (Figures S11 and S12). One reason for this is that regions with large differences in SNP densities between crosses were mainly located near centromeres where recombination is suppressed. However, even distal regions with high and different recombination rates among crosses, such as the regions of 0–2 Mb and 50–54 Mb on C5 of white × cauliflower and white × kohlrabi crosses (Figure S12), are not associated with major differences in SNP densities.

To investigate if SVs locally affect COs, we first focused on two inversions that were validated by Bionano optical maps (Cai et al., 2022); a 4.88-Mb kale-specific inversion in C3 and a 1.42-Mb cauliflower-specific inversion in C7 (Figure S13). We found only 1 CO inside this

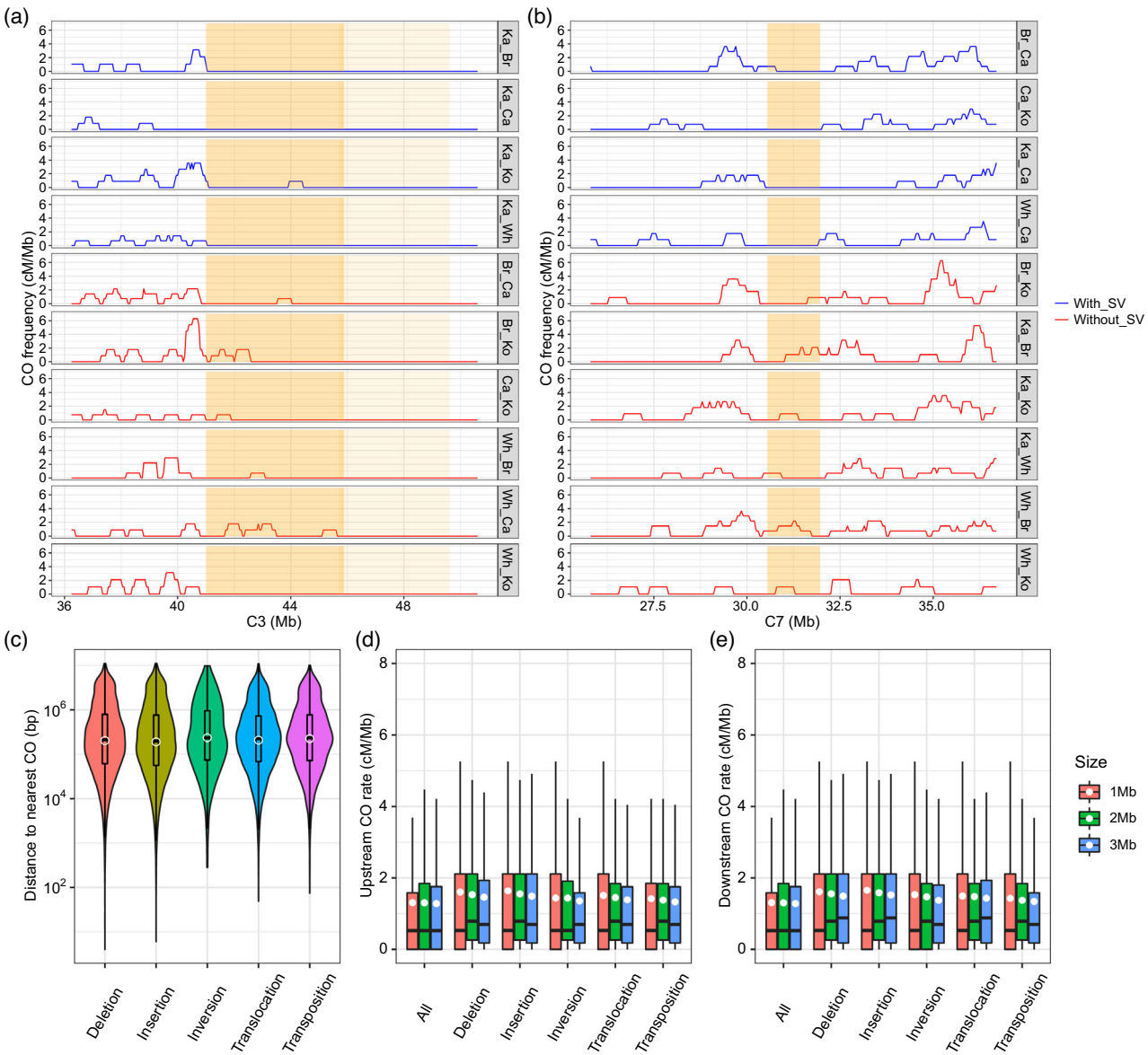

Figure 4. Effects of structural variations (SVs) on crossovers (COs).
(a) CO frequency in flanking regions of a 4.88-Mb kale specific inversion for the 10 sex-averaged crosses.
(b) CO frequency in flanking regions of a 1.42-Mb cauliflower specific inversion for the 10 sex-averaged crosses. Inversion and centromere regions are indicated by dark and light orange shadings, respectively. (a,b) CO frequency was calculated using 500-kb sliding windows with 50-kb step sizes. Br, broccoli; Ca, cauliflower; Ka, kale; Ko, kohlrabi; Wh, white cabbage.
(c) Distance of different types of SVs to their nearest CO, using the cross of Ka_Br as an example.
(d, e) Distributions of CO rates in windows of the indicated sizes in the (d) upstream and (e) downstream regions of different types of SVs, using the cross of Ka_Br as an example. "All" represents all windows genome-wide. (c–e) White dots indicate the average value.

region in crosses involving kale, while 13 COs were detected from crosses between parents lacking this inversion (Figure 4a). Similarly, we did not find any CO inside the 1.42-Mb cauliflower-specific inversion on C7 when crosses involved cauliflower, whereas 10 COs were observed inside this region in crosses between parents without this inversion (Figure 4b). To examine the local suppression effect on a broader scale, we compared all the SVs reported previously (Cai et al., 2022) (Table S4) against fine-resolution COs in the corresponding four crosses (Broccoli_Cauliflower, Broccoli_Kohlrabi, Kale_Broccoli and White_Broccoli). In all cases, occurrence of large deletions (≥500 bp) and inversions, translocations and transpositions independent of size translate into significantly reduced numbers of COs compared with expected by chance based on 5000 permutations (Figures S14–S17). However, short

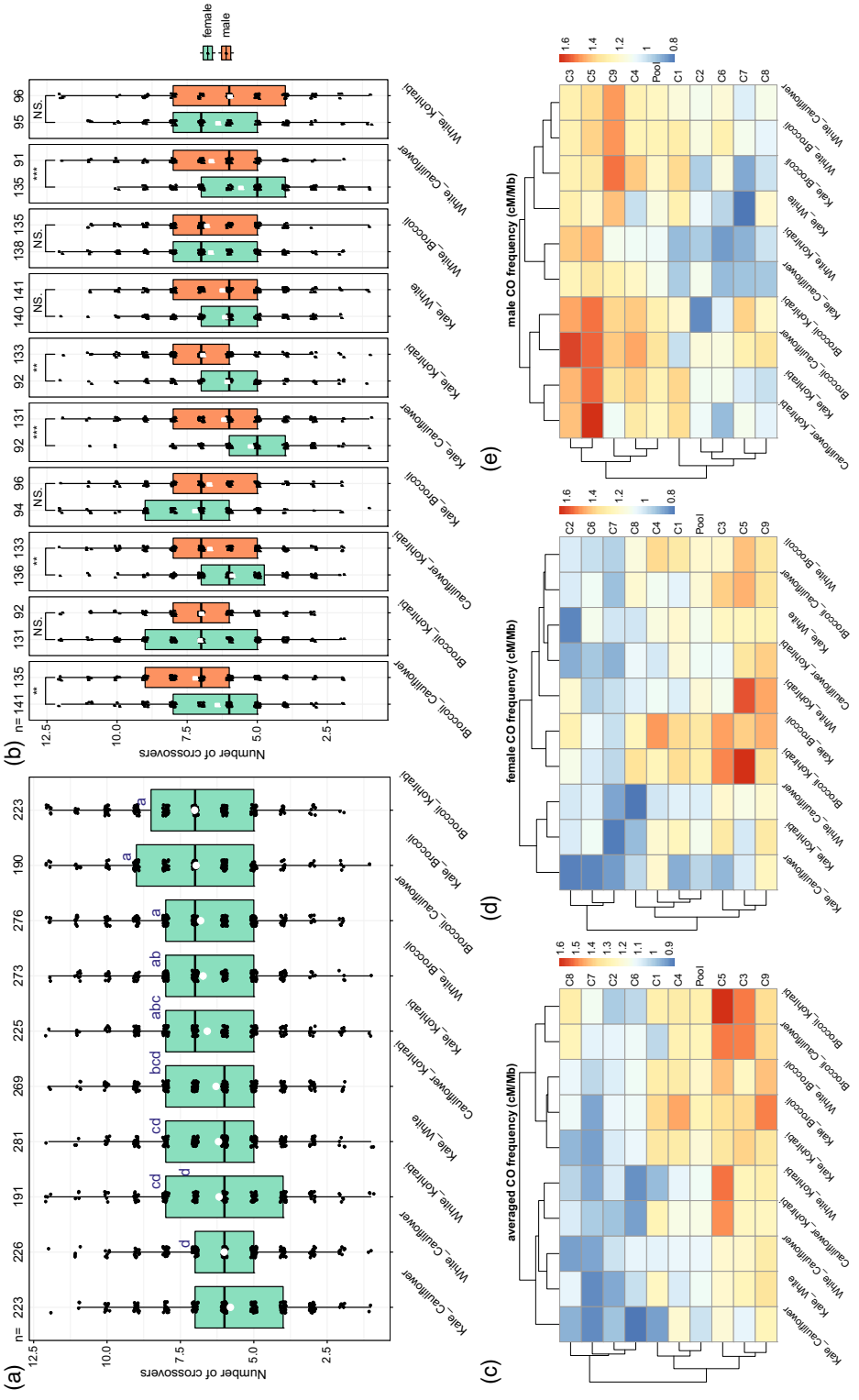

Figure 5. Crossover (CO) number variation and diversity of recombination frequency.
(a) Total number of COs per gamete shown for each of the 10 sex-averaged crosses. Multiple comparisons were performed using the Student–Newman–Keuls test with $a = 0.05$.
(b) Comparison of total number of COs per gamete between female and male meiosis for each cross. Asterisks indicate significant effects determined by Student's *t*-test ($P < 0.05$). (a, b) Each black dot represents a gamete of the given cross and the white dots indicate the average value.
(c–e) Heatmap of the chromosome-scale recombination rates measured for each chromosome in the 10 (c) sex-averaged, (d) female, and (e) male crosses. On the *y*-axis, "Pool" represents pooled analysis of all nine chromosomes.

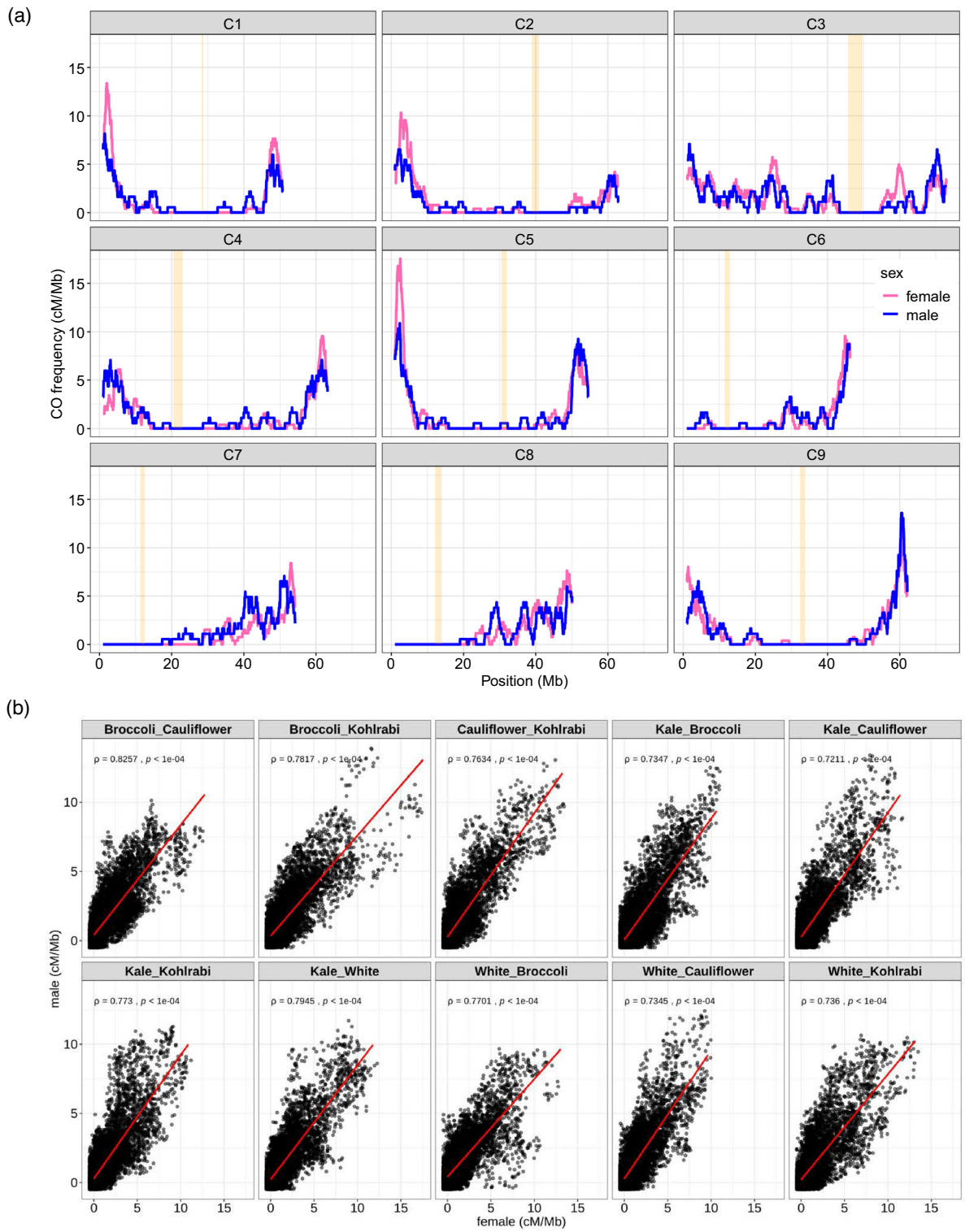

Figure 6. Comparison of recombination landscapes between female and male meiosis.
(a) Crossover (CO) distribution (window size 2 Mb, step size 50 kb) along the nine chromosomes in female and male meiosis of the cross of Broccoli_Kohlrabi.
(b) Correlation (Spearman's rank correlation) between female and male CO frequency in 2-Mb windows with 50-kb step size. Red lines indicate best fit and the shading areas represent the 95% confidence interval.

deletions (<500 bp) and insertions overlapped significantly more with CO sites than expected by chance.

While COs tend to be suppressed inside SVs, we investigated possible redistribution in flanking regions of SVs. SVs are spread all along chromosomes, and neither preferentially occur in distal arms nor in centromeric and pericentromeric regions (Figure S18). The SV distributions, however, differ between different genetic backgrounds. From the distribution of distance to the nearest CO for each SV, we found that in all four crosses investigated, inversions displayed the largest mean distance until their nearest CO in comparison with other types of SVs (Figure 4c; Figure S19; Table S4). We found the largest average distance to the nearest CO for all SVs in Broccoli_Kohlrabi (906.12–1316.71 kb), followed by Kale_Broccoli (690.90–856.84 kb), Broccoli_Cauliflower (651.76–749.37 kb) and White_Broccoli (575.04–668.61 kb) (Table S4), pointing to an effect of genetic background on the distance between SVs and their nearest CO. To test whether these distances are greater than expected by chance, we simulated random CO sites for the four crosses with each 10 000 times. The simulated mean distances ranged from 140.35 to 201.90 kb, all of which were significantly less than the observed distances (Table S4). Based on these findings, we conclude that CO suppression does not limit to SVs but also extends beyond their borders in *B. oleracea*. Interestingly, SV size has no effect on the distance to the nearest CO as revealed by correlation analyses (Spearman's rank correlation, ρ = –0.01 to 0.09) (Figure S20–S23). Regarding CO rates in the flanking 1-, 2- and 3-Mb upstream- and downstream regions of SVs, inversions showed lower average CO rates than the other SV types in nearly all cases, in agreement with larger distances to the nearest CO (Figure 4d,e; Figure S24). Inversions are not more interstitially localized than other types of SVs, but randomly distributed in the genome (Figure S18e). Thus, this lower average CO rates in flanking regions of inversions appears independent of the U-shaped CO distribution. The average CO rates in flanking regions of SVs were slightly higher than the observed genome-wide averages, implicating that loss of COs in SV regions is compensated by elevated COs in their flanking regions. Again, we found no correlation between SV size and CO rates in flanking regions (Spearman's rank correlation, ρ = –0.05 to 0.09), indicating that CO rates in the 1-Mb regions flanking SVs did not depend on their size (Figures S25–S28).

CO rate is shaped by cross combination, heterochiasmy, and their interactions

Our reciprocal FwC populations allowed us to examine CO variation between different cross combinations and between female versus male meiosis per genetic background. We first observed strong variation in CO rate among the 10 sex-averaged crosses, with the lowest average CO number per gamete in Kale_Cauliflower (5.80) and the highest in Broccoli_Kohlrabi (7.02) (Figure 5a). Based on the CO number distribution, the 10 sex-averaged crosses were classified into two groups: the "low CO rate" group, including Kale_Cauliflower, White_Cauliflower, White_Kohlrabi, Kale_White, and Cauliflower_Kohlrabi, and the "high CO rate" group including Broccoli_Kohlrabi, Kale_Broccoli, Broccoli_Cauliflower, White_Broccoli, and Kale_Kohlrabi. Within each group, no significant difference in CO number was observed between cross combinations (Student–Newman–Keuls test with a = 0.05). Four from the five crosses in the "high CO rate" group (all, except Kale_Kohlrabi) exhibited significantly more COs than four of five crosses in the "low CO rate" group (all except Cauliflower_Kohlrabi) (Student–Newman–Keuls test with a = 0.05). Interestingly, we found that generally fewer COs were produced when cauliflower and/or white cabbage were present in the cross combination. By contrast, the presence of broccoli in the background always resulted in higher CO numbers, even in crosses with cauliflower or white cabbage. Hierarchical clustering based on chromosome-wide sex-averaged recombination rates also revealed the abovementioned two groups, again indicating intraspecific variation of recombination rate in *B. oleracea* (Figure 5c). Chromosome-wide sex-averaged CO rates also varied among chromosomes, with higher recombination rates in C3, C5, and C9 than in C2, C6, C7, and C8. The intraspecific and chromosome-wide variations of recombination rate were also reflected in the sex-specific recombination rates (Figure 5d,e).

Interestingly, when comparing CO numbers between male and female meiosis, we highlighted marked differences, and thus heterochiasmy, according to the cross combinations analyzed. Indeed, significant variations were observed for five of the 10 cross combinations (Broccoli_Cauliflower, Cauliflower_Kohlrabi, Kale_Cauliflower, Kale_Kohlrabi, and White_Cauliflower), with always more COs formed during male than female meiosis (Figure 5b). Strikingly, variation in CO number between female and male gametes was always significant when cauliflower was involved in the cross combination. Together, this suggests that in *B. oleracea*, direction and combination of crosses are interdependent for CO variation. At chromosome scale, the average number of COs per chromatid was positively correlated with chromosome length in both sexes for all crosses (Spearman's rank correlation: 0.67–0.93, $P < 0.05$) (Figures S29 and S30), except for male meioses of Kale_Broccoli (P = 0.0503) and Kale_White (P = 0.0589). Despite these variations, Mb-scale recombination landscapes were remarkably conserved for the 10 sex-averaged and 20 sex-specific crosses, as well as between male and female meioses of each cross combination (Figure 6a; Figures S31–S33). Variations in CO numbers for genetic background and sex of meiosis were essentially

located on chromosome extremities that always exhibited the highest CO rates. Centromeres remained deprived of COs in all cases and pericentromeric regions showed the lowest CO frequencies and variations. The female and male recombination landscapes of each cross positively correlated with each other, with correlations in the range of 0.72–0.83 (Spearman's rank correlation, $P < 0.0001$) (Figure 6b). In both sexes, CO sites were enriched in gene bodies and their upstream and downstream 1-kb regions, whereas underrepresented in TE regions (Figure S34a). The distribution of distances between COs and genes was also similar between female and male gametes (Figure S34b). Moreover, the majority of COs formed per chromosome pair in both sexes were apart by large distances (50–55 Mb), independent of the cross combination (Figure S6b). We also observed the rare occurrence of multiple COs per chromatid in both sexes of all 10 crosses, with a deficit in gametes with 0 CO and an excess of gametes with 1 CO when comparing with the expected Poisson distributions (Figure S35). Together with our previous comparisons between cross combinations, these results indicate that CO interference intensity remains elevated, independently of the genetic background and the sex of meiosis in *B. oleracea*.

DISCUSSION

In the present study, we generated 10 female and 10 male CO maps in *B. oleracea*. To our knowledge, this is the first time that CO maps reached such a fine resolution in *Brassica* species. Besides maize, tomato, and potato, we expand the recombination knowledge to the economically important *B. oleracea* crops, which exhibit enormous phenotypic variations. More importantly, we included very diverse genetic backgrounds and reciprocal crosses, enabling the investigation of intraspecific variation, sex of meiosis, and their interaction on recombination in *B. oleracea*. To our knowledge, this is the most comprehensive study towards revealing intraspecific variation and sex differences of recombination rates and distributions. As meiotic recombination promotes genetic diversity by shuffling parental chromosomes, the present work provides insights towards improving breeding efficiency in *B. oleracea* via parental selection.

Recombination rate varies remarkably along chromosomes in *B. oleracea*; however, the Mb-scale landscapes are highly conserved between different genetic backgrounds. We observed preferential CO distribution towards distal regions in all *B. oleracea* crosses, consistent with those reported in related species, such as *B. rapa* (Pelé et al., 2017) and *B. napus* (Bayer et al., 2015; Boideau et al., 2022), as well as distant species such as potato (Marand et al., 2017), tomato (Demirci et al., 2017; Rommel Fuentes et al., 2020), maize (Kianian et al., 2018), and barley (Dreissig et al., 2020). We demonstrated that the Mb-scale *B. oleracea* U-shaped landscape is highly correlated with gene density. More interestingly, we observed several "CO bumps" that co-localize with elevated gene density. These observations indicate that gene density has a major contribution in shaping the Mb-scale recombination landscape in *B. oleracea*. In *A. thaliana*, Lian, Solier, Walkemeier, Huettel et al. (2022) also reported that gene density together with chromatin accessibility and DNA methylation could explain 85% of the Mb-scale recombination landscape using a machine-learning algorithm. This is in agreement with the strong positive correlations between CO distribution and gene density found in our study. Many epigenetic factors are reported to also affect the recombination frequency and distribution, with CO occurrence correlating with low levels of DNA methylation, low nucleosome density, and enrichment in specific histone marks. In this study, these hallmarks of open chromatin were not investigated. Generally, euchromatin is present in distal gene-rich regions and heterochromatin exists in large pericentromeric regions of the chromosome, which usually show a high level of DNA methylation and K3K9me2 histone marks (Boideau et al., 2022; Choulet et al., 2014; Li et al., 2019; Swagatika & Tomar, 2016). The U-shaped CO distribution we found in *B. oleracea* fits with the preferred occurrence of these epigenetic features. Nevertheless, the local influence of epigenetic factors on recombination in *B. oleracea* needs to be further analyzed to deepen our knowledge, as realized by Boideau et al. (2022), who investigated effects of methylation and SVs on the absence of recombination in *B. napus*. Both model-independent CO interference and KL divergence analysis validate strong CO interference in *B. oleracea*. However, the similar interference strengths indicated by KL divergence suggest weak influence of genetic background on CO interference (Table S2).

Small-scale sequence divergence can be both positively and negatively associated with recombination rate. We analyzed the level of SNPs from 2×2 comparisons between all parental genomes used in this study (Table S3). As in Arabidopsis (Blackwell et al., 2020), we also found parabolic relationships between SNP density and CO rate in all *B. oleracea* crosses. This is to some extent in agreement with the "juxtaposition effect" in Arabidopsis (Ziolkowski et al., 2015). The meiotic recombination is mutagenic, and this may increase polymorphism levels in regions with a high recombination rate. Aside from this, genetic hitchhiking and background selection tend to reduce genetic diversity in low recombination regions by increasing the frequency of beneficial mutations and eliminating deleterious mutations (Lian, Solier, Walkemeier, Huettel, et al., 2022; Ziolkowski et al., 2015). These are likely two reasons explaining the positive correlation between small-scale sequence divergence and recombination rate, given the hypothesis that polymorphisms are not

causal for the shape of the Mb-scale recombination landscape but rather the consequence (Lian, Solier, Walkemeier, Huettel, et al., 2022). The negative correlation is also expected because high levels of polymorphisms function such as large-scale genomic rearrangements, which do have local inhibitory effects on COs, as reported in Arabidopsis (Lian, Solier, Walkemeier, Huettel, et al., 2022; Rowan et al., 2019), tomato (Fuentes et al., 2022), *B. napus* (Boideau et al., 2022), and this study. We systematically investigated the impact of SV size and type on local recombination. This leads to our first conclusion that all types of large-scale SVs locally suppress recombination. We cannot totally exclude that a counter-selection of gametes exhibiting such events occurs as these would alter plants' viability (Rowan et al., 2019). A second conclusion is that SV size does not affect flanking CO rates and distance to nearest COs. Rowan et al. (2019) came up with several possible mechanisms explaining the underlying suppressive effects of SVs on COs, including the prevention of synaptonemal complex establishment, or reduction of DSB formation, or reduction of repairment from DSBs into COs. It is worth noting that we observed the enrichment of COs in short deletions (<500 bp) in our study, similar to that observed by Fuentes et al. (2022). This may be due to recombination resulting in short deletions instead of short deletions inducing more COs. Alternatively, this may suggest that small deletions do not suppress recombination. We found that large deletions (≥500 bp) overlapped significantly less with COs than expected by chance, confirming local suppression of large SVs on recombination (Figures S14–S17). For insertions, we would have expected similar patterns as for deletions, as analyzing insertions or deletions is just a matter of setting a reference. However, we can only find significantly more insertions overlapping with COs regardless of insertion size. As the sequence of an insertion is absent in the reference genome, we feel the overlap between CO interval and insertion loci is not accurate/realistic, and is likely influenced by the CO resolution.

Among the 10 cross combinations, we observed significant differences in CO number. Our data do not support that CO number and relatedness of parents are correlated. Indeed, we would expect higher numbers of COs when the two parents show higher levels of relatedness as a substrate with high homology may facilitate recombinational repair. However, this is not a general trend. For example, we observed a similar (not significantly different) average CO number in Kale_Broccoli (low level of relatedness) and Broccoli_Cauliflower (high level of relatedness). Interestingly, we found that the presence of broccoli in the parental combinations always results in a higher number of COs, even in crosses with cauliflower and white cabbage that were generally associated with lower number of COs (Figure 5a). Differences in CO rate have repeatedly been found according to the genetic background in plants. Recently, the study of loci affecting CO frequency has been made possible with the development of high-throughput technologies for measuring CO frequency from seeds in *A. thaliana* (Melamed-Bessudo et al., 2005; Ziolkowski et al., 2015). To date, three causal genes were identified: *HEI10*, *TAF4b*, and *SNI1* (Lawrence et al., 2019; Zhu et al., 2021; Ziolkowski et al., 2017). Accordingly, our data support a genetic control for CO rate via allelic variants segregating between the *B. oleracea* parental lines used in this study, with possible dominant allele(s) increasing CO rates in broccoli. While CO numbers varied, we did not identify major differences between the Mb-scale CO landscapes among our 10 cross combinations. CO variations were essentially located on chromosome extremities as observed between different populations of maize (Bauer et al., 2013). Accordingly, polymorphism in *HEI10*, *TAF4b*, and *SNI1* resulted in CO variation at chromosome extremities (Lawrence et al., 2019, Zhu et al., 2021, Ziolkowski et al., 2017). To date, the only natural factor associated with major changes in the shape of recombination landscapes, corresponds to variation in ploidy level. The most striking example arises in *Brassica* AAC allotriploids resulting from the cross between *B. napus* and its *B. rapa* progenitor. In these plants, an unprecedented boost of CO number was observed between A genomes and associated with the formation of COs in pericentromeric regions that are totally deprived of any recombination event in *B. rapa* and *B. napus* (Boideau et al., 2021; Pelé et al., 2017).

Comparison of female versus male meiosis for each of our 10 cross combinations revealed interdependency between heterochiasmy and genetic background. Indeed, half of the crosses showed significant variations, with higher recombination rates in male meiocytes. Our results contrast with a previous study conducted in *B. oleracea*, showing much more COs in female than male meiocytes (Kearsey et al., 1996). However, this study was based on 75 molecular markers, affecting the reliability. Importantly, our data support observations made in maize for which B73 × Mo17 and Zheng58 × SK backgrounds result in the absence and presence of heterochiasmy, respectively (Kianian et al., 2018; Luo et al., 2019). In their study, Luo et al. (2019) suggested that the occurrence of CO maturation inefficiency (CMI), which will block some designated COs developing into actual COs, differs between genetic backgrounds and between sexes in maize. CMI was indeed detected in maize in both male and female meiosis within the B73 × Mo17 background and in male meiosis of the inbred line KYS, but not in the Zheng58 × SK background (Luo et al., 2019). This corroborates with our observations as higher CO rates were always observed in male versus female meiosis when cauliflower was involved in the cross combination. One possible explanation for not detecting heterochiasmy in other combinations tested is that CMI is a recessive trait that does not exist in cauliflower.

Alternative explanations for observed heterochiasmy in all cross combinations with cauliflower is a dominant locus in cauliflower promoting increased CO rates exclusively during pollen grain formation but not in female meiosis. This locus may influence synapsis progression during male meiosis, the length of which is positively related to CO number in both sexes as observed in maize (Luo et al., 2019). Despite the heterochiasmy, we observed fairly similar CO distribution between male and female meiocytes. This observation in *B. oleracea* is consistent with that in maize (Kianian et al., 2018); however, it is remarkably different with that in *A. thaliana* (Lian, Solier, Walkemeier, Huettel, et al., 2022).

In conclusion, we generated high resolution recombination landscapes, improving our knowledge of CO formation in *B. oleracea*, and showed remarkable CO variation depending on the direction and combination of the cross, which is highly relevant for breeders.

EXPERIMENTAL PROCEDURES

FwC population construction, DNA isolation and sequencing

We previously *de novo* assembled genome sequences for five *B. oleracea* accessions, representing five diverse morphotypes, by integrating Nanopore long reads, optical mapping molecules (BioNano Genomics DLS Technology, San Diego, CA, USA) and Illumina short reads (Cai et al., 2022). We generated chromosome-scale genome assemblies, with contig N50s ranging from 11.4 to 16.3 Mb and scaffold N50s ranging from 30.5 to 34.1 Mb. The complete BUSCO values were greater than 97% for all the five assemblies using BUSCO (embryophyta_odb9 dataset, n = 1440) assessment. In this study, we used these five DH lines (broccoli, cauliflower, kale, kohlrabi, and white cabbage) as founders to construct FwC populations to study the inter-morphotype recombination landscape (Figure S1). These five founders were pairwise crossed to generate 10 F1s, after which the 10 F1s were intercrossed to generate large FwC populations. To observe recombination between each combination of the five morphotypes, we constructed five FwC populations with each containing four different parents (Figure 1). We reciprocally crossed the two F1 plants for each FwC population, resulting in 10 populations that allow us to study female and male COs for each of the 10 crosses.

Genomic DNA was isolated from young leaves of the five FwC population plants using a cetyltrimethylammonium bromide method (Allen et al., 2006). Libraries were constructed with the RipTide DNA library prep kit (iGenomX, Carlsbad, CA, USA), which is designed for the preparation of 96 next-generation sequencing DNA libraries at a time. We collected a total of 1248 plants from the five FwC populations (Figure 1). Individual samples were labeled in thirteen 96-well plates, after which samples per plate were pooled together and converted into a NGS library in one single tube. The 13 pooled libraries were respectively sequenced as 150 bp paired-end reads using Illumina NovaSeq 6000.

Read processing, SNP calling and filtering

FGBIO DEMUXFASTQS (v1.1.0) was used to demultiplex samples per plate according to sample barcodes provided by iGenomX. In total, 47 samples (Table S1) each with less than 100 Mb (approximately 0.18×) sequencing data were excluded from downstream analyses. All reads from each sample were aligned to the broccoli reference genome (Cai et al., 2022) using BWA-MEM (v0.7.15) (Li & Durbin, 2009) with default parameters. SAMtools (v1.3.1) (Li et al., 2009) was used to perform sorting of the alignments. The function of HaplotypeCaller in Genome Analysis Toolkit (GATK, v4.1.7.0) (McKenna et al., 2010) was used to produce GVCF files on a per-sample basis, before which duplicated, secondary alignment reads and reads with low mapping quality were filtered out using default settings. We used the CombineGVCF function in GATK to combine per-sample GVCF files into a single GVCF file for each of the 10 reciprocal populations, following which the GenotypeGVCF function was used to perform the joint genotyping. The SelectVariant function was then used to select biallelic SNPs and further SNP filtering was performed using the VariantFiltration function with parameters "--filter-expression 'QD < 2.0 || FS > 60.0 || MQ < 40.0' --cluster-window-size 5 --cluster-size 2 --filter-name LowQual." SNPs among the five parental lines were called using the high-depth Illumina sequencing data generated by (Cai et al., 2022) with similar strategies as described above for the populations. Only homozygous parental SNPs were retained.

Detection of CO

Given the FwC strategy in this study, we selected parental SNPs, which allow us to identify COs that occurred for each combination of the five parents. To identify COs between P1 and P2, we selected parental SNPs in which we only allow genotype variations between these two parents while not between the other two parents (P3 and P4) (Figure S36). Similarly, to detect COs between P3 and P4, we selected another group of SNPs in which we allow genotype variations between P3 and P4 while not between P1 and P2. The selected parental SNPs were intersected with the SNP matrix of the corresponding population. SNP sites with more than 40% missing genotype calls were discarded. The parental origin for the allele at each SNP site was inferred based on the observed genotypes for the four parents and the FwC progeny. The chi-squared test for goodness of fit was used to analyze segregation distortions. The expected segregation ratio is 1:1. SNP sites with significant segregation distortion at a significance level of P = 0.001 were removed from further analysis. As SNPs in close proximity in physical maps are supposed to be highly linked in biparental populations (Marand et al., 2017, 2019), SNPs demonstrating low levels of LD with neighboring markers are likely false-positive variants. We thus estimated local r^2 values for each SNP using the nearest 100 SNPs to determine associated alleles and removed SNPs with local r^2 values <0.3 (mean r^2 values across the 100 comparisons).

PhaseLD (Marand et al., 2017) (https://github.com/plantformatics/phaseLD) was then used to reconstruct the haplotype phase with parameters "--quick_mode --win 100 --bwin 200 --bstep 5 --rpen 0.3." This pipeline implemented a sliding window approach to overcome sequencing and genotyping errors that could arise from assembly errors or SVs. We applied 200-SNP sliding windows with five SNP steps to estimate the posterior probability of both haplotypes using Bayes theorem for each individual in a given window. The haplotype with the highest probability was called for the given window. Putative COs were determined from these overlapping adjacent haplotype bins. Precise CO breakpoints were then identified using the logistic regression approach as implemented in "extract_crossovers.pl" (https://github.com/plantformatics/phaseLD/tree/master/bin), which assigns CO probabilities to each SNP. To reduce false positive CO counts, only the pair of SNPs with a CO probability greater than

0.9 were kept as the identified CO intervals. To remove further the likely false positive COs, CO positions that appeared to be double COs <2 Mb apart were removed. We employed all these steps to minimize the risk of false CO detection, keeping in mind that true CO numbers should be similar to those reported in other *Brassica* populations (0.70–0.92 CO occurrences on average per chromatid) (Boideau et al., 2022; Pelé et al., 2017).

CO number and landscape analyses

We calculated three-fold interquartile ranges for the 10 reciprocal crosses using TCN of each gamete. Gametes with TCN outside the three-fold interquartile range (0.5–12.5) were removed, like done in other studies (Dreissig et al., 2020). Compared with the population mean of 6.57 and outlier-pruned mean of 6.49, these outliers (22 of 2399 gametes) showed a mean TCN of 15.09 (Table S5). We calculated Poisson distributions of CO number per chromatid per gamete using the following formula: $S(k) = N(e^{-m}m^k/k!)$ where $S(k)$ is the number of gametes harboring exactly k CO, N is the total number of gametes, m is the observed mean number of CO per gamete, and e is the natural logarithm base (Drouaud et al., 2007; Giraut et al., 2011). Recombination landscapes of each chromosome of each cross were visualized using 2 Mb sliding windows with 50 kb steps. We summarized CO frequency (cM per Mb) as $C/n/(w/10^6) \times 100$, where w is the window size, C is the number of recombinant gamete in the given window, and n is the total number of gametes for the population (Campoy et al., 2020; Dreissig et al., 2020).

Inference of putative centromeric and pericentromeric regions

Centromeric regions were determined using the approach described by Cheng et al. (2013) and Cai et al. (2020). Briefly, centromere-specific repeat sequences, such as CentBr, CRB, and TR238 (Koo et al., 2004, 2011; Lim et al., 2005, 2007), were aligned to the broccoli reference genome using nucmer with parameters "--maxmatch -g 500 -c 16 -l 16" (Marçais et al., 2018). Centromeric regions were located based on the distribution of these elements in the reference genome (Table S6). Thereafter, the broccoli genome and *B. napus* cv. Darmor-bzh v10 C-genome (Rousseau-Gueutin et al., 2020) were aligned to identify syntenic regions using SyRI (Goel et al., 2019). The closest syntenic regions to each border of *B. napus* cv. Darmor-bzh v10 C-genome pericentromeres, which were defined by (Boideau et al., 2022), were extracted from the *B. napus* genome. The corresponding regions in the broccoli genome were then defined as the borders for the putative pericentromeric regions (Table S6).

Association analyses between genomic features and COs

To investigate CO interference, we calculated distances between adjacent COs for each gamete per chromatid having at least two COs, using the mid-value of the positions of the two CO flanking markers. The observed interference distributions were compared with no-interference distributions, obtained using a randomly shuffling approach proposed by Pelé et al. (2017). COs at fine-resolution (less than 10 kb) were selected to analyze the overlap (minimum 1 bp) with various genomic features (exons, introns, 1 kb upstream and downstream gene regions, TEs, and intergenic regions) (Marand et al., 2017). Random genomic regions were permuted 10 000 times using BEDtools shuffle (v2.27.1) (Quinlan & Hall, 2010), and were then assessed for overlap with each genomic feature. SNP densities between each combination of the parents were calculated using 2 Mb sliding windows with 50 kb steps. The positions of SVs between parental genomes were obtained from Cai et al. (2022). Overlaps between fine-resolution CO intervals and the SV regions were studied using regioneR (Gel et al., 2016). We performed another 10 000 times of Monte Carlo simulation using BEDTOOLS SHUFFLE (v2.27.1) to generate random genomic sequences matched by number and length to the CO dataset from the broccoli reference genome. Thereafter, we searched for the nearest simulated genomic sequence from each simulation in the flanking regions of each SV, and calculated the distance between each of the two SV borders and the nearest simulated region. We took the smaller value as the distance to the nearest simulated region for each SV. We then compared this expected distance distribution with the observed distribution that was obtained using the real CO dataset. CO rates in 1-, 2-, and 3-Mb upstream and downstream of the borders for SVs were calculated and were compared with the genome-wide level CO rates.

AUTHOR CONTRIBUTIONS

GB and CC designed the research. JB performed the wet lab experiments. CC, AP, and RF analyzed data. CC drafted the manuscript. CC, AP, and GB revised the manuscript. All authors read and approved the final manuscript.

ACKNOWLEDGEMENTS

We would like to thank Theo Borm, Hans de Jong, Korbinian Schneeberger, and Roven Rommel Fuentes for helpful discussions. We thank Fernanda de Alves Freitas Guesdes for the try-out data analysis. This research was funded by the TKI project KV 1605-004 "A *de novo* sequencing catalogue *B. oleracea*" (https://topsectortu.nl/nl/de-novo-sequencing-catalogue-b-oleracea), and was co-supported by two breeding companies (Bejo and ENZA). CC is supported by China Scholarship Council (no. 201809110159).

CONFLICT OF INTEREST

The authors declare that they have no competing interests.

DATA AVAILABILITY STATEMENT

The raw sequencing reads for the 5 four-way-cross (FwC) populations in this study have been deposited in NCBI under the accession number PRJNA847181. List of CO positions identified for each reciprocal cross can be found in Table S7.

SUPPORTING INFORMATION

Additional Supporting Information may be found in the online version of this article.

Figure S1. Illustration of the five parental *Brassica oleracea* genotypes used for four-way-cross (FwC) population construction and the 10 F1s generated by pairwise crosses.

Figure S2. Distribution of segregating SNPs, which were used for crossover (CO) detection, along the nine chromosomes of *Brassica oleracea* for each of the 10 reciprocal crosses.

Figure S3. Haplotype map of the 10 reciprocal crosses. Orange and blue segments reflect the two parental alleles segregating in the corresponding population.

Figure S4. Distribution of total crossover (CO) number per gamete across the 2377 gametes in the 10 reciprocal crosses.

Figure S5. Distribution of crossover (CO) numbers per chromatid in the 10 sex-averaged crosses. (a) Observed distributions. (b)

Expected Poisson distributions (see "Experimental procedures" section).

Figure S6. Distribution of inter-crossover (CO) distance for chromatids having at least two COs. (a) Comparison of inter-CO distance distribution among the 10 sex-averaged crosses. Solid lines indicate the observed data. Dashed lines correspond to the corresponding distributions in the shuffled data ("non-interference" situation), as was described in "Experimental procedures." (b) Comparison of inter-CO distance distribution between female and male meiosis in each cross.

Figure S7. Sliding window-based recombination landscapes (window size 2 Mb, step size 50 kb) for the 10 sex-averaged crosses. Centromere regions are indicated by orange shadings.

Figure S8. Permutation tests for evaluating overlaps between genes and crossover (CO) intervals for all the 10 reciprocal crosses. Female and male meioses are indicated in the left and right column, respectively. On *x*-axis, the values are the total number of overlaps. On *y*-axis, the values are the frequency. Vertical red lines indicate the number of overlaps where $P = 0.05$. Vertical green lines indicate the observed number of overlaps. Vertical black lines indicate the mean of 5000 permutations. Double arrow highlights the difference between the mean and the observed values.

Figure S9. Normalized distribution of crossovers (COs) in the 10 sex-averaged crosses and of SNP density between each pair of parents along the nine chromosomes of *Brassica oleracea*. Analysis is done with 2-Mb sliding windows and 50-kb step sizes. CO frequency was normalized to range from 0 (min) to 1 (max) and SNP density was normalized to range from −1 (min) to 0 (max). The centromere regions are indicated by orange shadings.

Figure S10. Correlation (Spearman's rank correlation) between crossover (CO) frequency and SNP density in 2-Mb sliding windows with 50-kb step sizes for each sex-averaged cross. (a) Correlation analysis with pericentromeric regions being included. (b) Correlation analysis with pericentromeric regions being excluded. Trend lines were generated using a generalized additive model (GAM) with the formula *y* approximately poly(*x*,2). Vertical blue lines represent mean SNP density (the number of SNPs per 2-Mb window).

Figure S11. Crossover (CO) distribution comparison between the cross of Broccoli_Cauliflower and White_Cauliflower, and the corresponding parental SNP density distribution comparison. Analysis is done with 2-Mb sliding windows and 50-kb step sizes. The centromeric and pericentromeric regions are indicated by dark and light orange shadings, respectively. Asterisks indicate intervals (non-overlapping 2-Mb windows) with significant CO frequency difference between the two crosses ($P < 0.05$, chi-squared test).

Figure S12. Crossover (CO) distribution comparison between the cross of White_Cauliflower and White_Kohlrabi, and the corresponding parental SNP density distribution comparison. Analysis is done with 2-Mb sliding windows and 50-kb step sizes. Centromeric and pericentromeric regions are indicated by dark and light orange shadings, respectively. Asterisks indicate intervals (non-overlapping 2-Mb windows) with significant CO frequency difference between the two crosses ($P < 0.05$, chi-squared test).

Figure S13. Bionano evidence for two large inversions. (a) A 4.88-Mb kale-specific inversion on chromosome C3. (b) A 1.42-Mb cauliflower-specific inversion on chromosome C7.

Figure S14. Permutation tests for evaluating overlaps between different types of structural variations (indicated in the top right corner of each figure) and crossover (CO) intervals for the cross of Broccoli_Cauliflower. On the *x*-axis, the values are the total number of overlaps. On the *y*-axis, the values are the frequency. Vertical red lines indicate the number of overlaps where $P = 0.05$. Vertical green lines indicate the observed number of overlaps. Vertical black lines indicate the mean of 5000 permutations. Double arrow highlights the difference between the mean and the observed values.

Figure S15. Permutation tests for evaluating overlaps between different types of structural variations (indicated in the top right corner of each figure) and crossover (CO) intervals for the cross of Broccoli_Kohlrabi. On the *x*-axis, the values are the total number of overlaps. On the *y*-axis, the values are the frequency. Vertical red lines indicate the number of overlaps where $P = 0.05$. Vertical green lines indicate the observed number of overlaps. Vertical black lines indicate the mean of 5000 permutations. Double arrow highlights the difference between the mean and the observed values.

Figure S16. Permutation tests for evaluating overlaps between different types of structural variations (indicated in the top right corner of each figure) and crossover (CO) intervals for the cross of Kale_Broccoli. On the *x*-axis, the values are the total number of overlaps. On the *y*-axis, the values are the frequency. Vertical red lines indicate the number of overlaps where $P = 0.05$. Vertical green lines indicate the observed number of overlaps. Vertical black lines indicate the mean of 5000 permutations. Double arrow highlights the difference between the mean and the observed values.

Figure S17. Permutation tests for evaluating overlaps between different types of structural variations (indicated in the top right corner of each figure) and crossover (CO) intervals for the cross of White_Broccoli. On the *x*-axis, the values are the total number of overlaps. On the *y*-axis, the values are the frequency. Vertical red lines indicate the number of overlaps where $P = 0.05$. Vertical green lines indicate the observed number of overlaps. Vertical black lines indicate the mean of 5000 permutations. Double arrow highlights the difference between the mean and the observed values.

Figure S18. Distribution of structural variations (SVs) for four morphotypes relative to the broccoli reference genome. (a–d) Number of SVs in 2-Mb windows with 50-kb steps for deletions, insertions, translocations, and transpositions, respectively. (e) Distribution of inversions along the chromosomes. For large inversions (≥10 000 bp), the size of each segment corresponds to the size of the inversion. However, to show small inversions (<10 000 bp) in the figure, we reset their size as 10 000 bp. Centromere regions are indicated by orange shadings.

Figure S19. Violin plot of distance to the nearest crossover (CO) for different types of structural variations (SVs). White dots indicate average values. Vertical rectangles indicate the interquartile ranges.

Figure S20. Correlation (Spearman's rank correlation) between the size of structural variations (SVs) (broccoli versus cauliflower genome) and the distance to their nearest crossover (CO) (Broccoli_Cauliflower cross). Type of SVs is indicated in the top right corner of each figure.

Figure S21. Correlation (Spearman's rank correlation) between the size of structural variations (SVs) (broccoli versus kohlrabi genome) and the distance to their nearest crossover (CO) (Broccoli_Kohlrabi cross). Type of SVs is indicated in the top right corner of each figure.

Figure S22. Correlation (Spearman's rank correlation) between the size of structural variations (SVs) (broccoli versus kale genome) and the distance to their nearest crossover (CO) (Kale_Broccoli cross). Type of SVs is indicated in the top right corner of each figure.

Figure S23. Correlation (Spearman's rank correlation) between the size of structural variations (SVs) (broccoli versus white cabbage genome) and the distance to their nearest crossover (CO) (White_Broccoli cross). Type of SVs is indicated in the top right corner of each figure.

Figure S24. Distribution of crossover (CO) rates in windows of the indicated sizes in the (a) upstream and (b) downstream regions of different types of structural variations (SVs). "All" represents all windows genome-wide. White dots indicate the average values.

Figure S25. Correlation (Spearman's rank correlation) between the size of structural variations (SVs) (broccoli versus cauliflower genome) and the crossover (CO) rates (Broccoli_Cauliflower cross) in their flanking 1-Mb regions.

Figure S26. Correlation (Spearman's rank correlation) between the size of structural variations (SVs) (broccoli versus kohlrabi genome) and the crossover (CO) rates (Broccoli_Kohlrabi cross) in their flanking 1-Mb regions.

Figure S27. Correlation (Spearman's rank correlation) between the size of structural variations (SVs) (broccoli versus kale genome) and the crossover (CO) rates (Kale_Broccoli cross) in their flanking 1-Mb regions.

Figure S28. Correlation (Spearman's rank correlation) between the size of structural variations (SVs) (broccoli versus white cabbage genome) and the crossover (CO) rates (White_Broccoli cross) in their flanking 1-Mb regions.

Figure S29. Mean number of crossovers (COs) per chromatid along the nine chromosomes of *Brassica oleracea* for the sex-averaged, female and male crosses. On the *x*-axis, chromosomes were ordered according to their lengths.

Figure S30. Correlation (Spearman's rank correlation) between chromosome length and mean crossover (CO) number per chromatid. (a) Correlation analysis for each of the 10 sex-averaged, female or male crosses. (b) Correlation analysis based on the pool of 10 sex-averaged, female or male crosses.

Figure S31. Recombination landscapes for the 10 female crosses. (a) Crossover (CO) rate distributions along the nine chromosomes of *Brassica oleracea*. Analysis is done with 2-Mb sliding windows and 50-kb step sizes. Centromere regions are indicated by orange shadings. (b) Genome-wide correlation coefficient (Spearman's rank correlation) matrices among the 10 female CO distributions.

Figure S32. Recombination landscapes for the 10 male crosses. (a) Crossover (CO) rate distributions along the nine chromosomes of *Brassica oleracea*. Analysis is done with 2-Mb sliding windows and 50-kb step sizes. Centromere regions are indicated by orange shadings. (b) Genome-wide correlation coefficient (Spearman's rank correlation) matrices among the 10 male CO distributions.

Figure S33. Crossover (CO) distribution (window size 2 Mb, step size 50 kb) along the nine chromosomes in female and male meiosis of nine crosses. For the cross of Broccoli_Kohlrabi, see Figure 6. Centromere regions are indicated by orange shadings.

Figure S34. Genomic features associated with female and male meiotic crossovers (COs). (a) Overlap analysis of female and male COs with different genomic features. (b) Distribution of distance from each CO to the nearest gene. (a) CO interval was used for the overlap analysis. If an interval overlapped with multiple genomic features, the interval was counted towards each genomic feature. (b) Middle position of both CO interval and gene was used for calculating the distance.

Figure S35. Comparison of crossover (CO) number distributions per chromatid between female and male meiosis for all 10 cross combinations. Observed and expected CO number distributions were also compared. 'Expected distribution' denotes Poisson distribution (see "Experimental procedures" section).

Figure S36. Parental SNPs selection for crossover (CO) identification (see "Experimental procedures" section). This example shows how parental SNPs were selected to identify COs that occur between P1 and P2. Only genotype variations between P1 and P2 are allowed. Parental origin can be inferred based on the genotype of parents and FwC progenies.

Table S1. Illumina sequencing data for each progeny of the 5 four-way-cross (FwC) populations.

Table S2. Quantitative measurement of interference strength based on the Kullback–Leibler (KL) divergence from the observed to the "no-interference" distribution (see "Experimental procedures" section).

Table S3. Number of SNPs between each pair of the five parental genomes.

Table S4. Statistics of structural variations (SVs) and the distance to their nearest crossover (CO).

Table S5. Three-fold interquartile range of total crossover (CO) number per gamete.

Table S6. Inferred positions of the centromeric and pericentromeric regions for the nine broccoli chromosomes.

Table S7. List of crossover (CO) positions identified for each of the 10 reciprocal crosses.

REFERENCES

Alhajturki, D., Muralidharan, S., Nurmi, M., Rowan, B.A., Lunn, J.E., Boldt, H. *et al.* (2018) Dose-dependent interactions between two loci trigger altered shoot growth in BG-5 × Krotzenburg-0 (Kro-0) hybrids of *Arabidopsis thaliana*. *New Phytologist*, **217**, 392–406.

Allen, G.C., Flores-Vergara, M., Krasynanski, S., Kumar, S. & Thompson, W. (2006) A modified protocol for rapid DNA isolation from plant tissues using cetyltrimethylammonium bromide. *Nature Protocols*, **1**, 2320–2325.

Anderson, L.K., Lai, A., Stack, S.M., Rizzon, C. & Gaut, B.S. (2006) Uneven distribution of expressed sequence tag loci on maize pachytene chromosomes. *Genome Research*, **16**, 115–122.

Bauer, E., Falque, M., Walter, H., Bauland, C., Camisan, C., Campo, L. *et al.* (2013) Intraspecific variation of recombination rate in maize. *Genome Biology*, **14**, 1–17.

Bayer, P.E., Ruperao, P., Mason, A.S., Stiller, J., Chan, C.-K.K., Hayashi, S. *et al.* (2015) High-resolution skim genotyping by sequencing reveals the distribution of crossovers and gene conversions in *Cicer arietinum* and *Brassica napus*. *Theoretical and Applied Genetics*, **128**, 1039–1047.

Begun, D.J. & Aquadro, C.F. (1992) Levels of naturally occurring DNA polymorphism correlate with recombination rates in *D. melanogaster*. *Nature*, **356**, 519–520.

Blackwell, A.R., Dluzewska, J., Szymanska-Lejman, M., Desjardins, S., Tock, A.J., Kbiri, N. *et al.* (2020) MSH 2 shapes the meiotic crossover landscape in relation to interhomolog polymorphism in Arabidopsis. *The EMBO Journal*, **39**, e104858.

Boideau, F., Pelé, A., Tanguy, C., Trotoux, G., Eber, F., Maillet, L. *et al.* (2021) A modified meiotic recombination in *Brassica napus* largely improves its breeding efficiency. *Biology*, **10**, 771.

Boideau, F., Richard, G., Coriton, O., Huteau, V., Belser, C., Deniot, G. *et al.* (2022) Epigenomic and structural events preclude recombination in *Brassica napus*. *New Phytologist*, **234**, 545–559.

Cai, C., Bucher, J., Finkers, R. & Bonnema, G. (2022) Chromosome-scale genome assemblies of five different *Brassica oleracea* morphotypes provide insights in intraspecific diversification. *bioRxiv*. Available from: https://doi.org/10.1101/2022.10.27.514037

Cai, X., Wu, J., Liang, J., Lin, R., Zhang, K., Cheng, F. *et al.* (2020) Improved *Brassica oleracea* JZS assembly reveals significant changing of LTR-RT dynamics in different morphotypes. *Theoretical and Applied Genetics*, **133**, 3187–3199.

Campoy, J.A., Sun, H., Goel, M., Jiao, W.-B., Folz-Donahue, K., Wang, N. *et al.* (2020) Gamete binning: chromosome-level and haplotype-resolved

genome assembly enabled by high-throughput single-cell sequencing of gamete genomes. *Genome Biology*, **21**, 1–20.

Capilla-Pérez, L., Durand, S., Hurel, A., Lian, Q., Chambon, A., Taochy, C. *et al.* (2021) The synaptonemal complex imposes crossover interference and heterochiasmy in Arabidopsis. *Proceedings of the National Academy of Sciences of the United States of America*, **118**, e2023613118.

Cheng, F., Mandáková, T., Wu, J., Xie, Q., Lysak, M.A. & Wang, X. (2013) Deciphering the diploid ancestral genome of the mesohexaploid *Brassica rapa*. *The Plant Cell*, **25**, 1541–1554.

Choi, K., Zhao, X., Kelly, K.A., Venn, O., Higgins, J.D., Yelina, N.E. *et al.* (2013) Arabidopsis meiotic crossover hot spots overlap with H2A. Z nucleosomes at gene promoters. *Nature Genetics*, **45**, 1327–1336.

Choi, K., Zhao, X., Tock, A.J., Lambing, C., Underwood, C.J., Hardcastle, T.J. *et al.* (2018) Nucleosomes and DNA methylation shape meiotic DSB frequency in *Arabidopsis thaliana* transposons and gene regulatory regions. *Genome Research*, **28**, 532–546.

Choulet, F., Alberti, A., Theil, S., Glover, N., Barbe, V., Daron, J. *et al.* (2014) Structural and functional partitioning of bread wheat chromosome 3B. *Science*, **345**, 1249721.

Coop, G. & Przeworski, M. (2007) An evolutionary view of human recombination. *Nature Reviews Genetics*, **8**, 23–34.

Crismani, W., Girard, C., Froger, N., Pradillo, M., Santos, J.L., Chelysheva, L. *et al.* (2012) FANCM limits meiotic crossovers. *Science*, **336**, 1588–1590.

Cutter, A.D. & Payseur, B.A. (2013) Genomic signatures of selection at linked sites: unifying the disparity among species. *Nature Reviews Genetics*, **14**, 262–274.

De Muyt, A., Mercier, R., Mezard, C. & Grelon, M. (2009) Meiotic recombination and crossovers in plants. *Meiosis*, **5**, 14–25.

Demirci, S., van Dijk, A.D., Sanchez Perez, G., Aflitos, S.A., de Ridder, D. & Peters, S.A. (2017) Distribution, position and genomic characteristics of crossovers in tomato recombinant inbred lines derived from an interspecific cross between *Solanum lycopersicum* and *Solanum pimpinellifolium*. *The Plant Journal*, **89**, 554–564.

Dooner, H.K. & He, L. (2008) Maize genome structure variation: interplay between retrotransposon polymorphisms and genic recombination. *The Plant Cell*, **20**, 249–258.

Dreissig, S., Mascher, M. & Heckmann, S. (2019) Variation in recombination rate is shaped by domestication and environmental conditions in barley. *Molecular Biology and Evolution*, **36**, 2029–2039.

Dreissig, S., Maurer, A., Sharma, R., Milne, L., Flavell, A.J., Schmutzer, T. *et al.* (2020) Natural variation in meiotic recombination rate shapes introgression patterns in intraspecific hybrids between wild and domesticated barley. *New Phytologist*, **228**, 1852–1863.

Drouaud, J., Mercier, R., Chelysheva, L., Bérard, A., Falque, M., Martin, O. *et al.* (2007) Sex-specific crossover distributions and variations in interference level along *Arabidopsis thaliana* chromosome 4. *PLoS Genetics*, **3**, e106.

Erayman, M., Sandhu, D., Sidhu, D., Dilbirligi, M., Baenziger, P. & Gill, K.S. (2004) Demarcating the gene-rich regions of the wheat genome. *Nucleic Acids Research*, **32**, 3546–3565.

Feldman, M.W., Otto, S.P. & Christiansen, F.B. (1996) Population genetic perspectives on the evolution of recombination. *Annual Review of Genetics*, **30**, 261–295.

Fuentes, R.R., de Ridder, D., van Dijk, A.D. & Peters, S.A. (2022) Domestication shapes recombination patterns in tomato. *Molecular Biology and Evolution*, **39**, msab287.

Gel, B., Diez-Villanueva, A., Serra, E., Buschbeck, M., Peinado, M.A. & Malinverni, R. (2016) regioneR: an R/Bioconductor package for the association analysis of genomic regions based on permutation tests. *Bioinformatics*, **32**, 289–291.

Giraut, L., Falque, M., Drouaud, J., Pereira, L., Martin, O.C. & Mézard, C. (2011) Genome-wide crossover distribution in *Arabidopsis thaliana* meiosis reveals sex-specific patterns along chromosomes. *PLoS Genetics*, **7**, e1002354.

Goel, M., Sun, H., Jiao, W.-B. & Schneeberger, K. (2019) SyRI: finding genomic rearrangements and local sequence differences from whole-genome assemblies. *Genome Biology*, **20**, 1–13.

Gore, M.A., Chia, J.-M., Elshire, R.J., Sun, Q., Ersoz, E.S., Hurwitz, B.L. *et al.* (2009) A first-generation haplotype map of maize. *Science*, **326**, 1115–1117.

Habu, Y., Ando, T., Ito, S., Nagaki, K., Kishimoto, N., Taguchi-Shiobara, F. *et al.* (2015) Epigenomic modification in rice controls meiotic recombination and segregation distortion. *Molecular Breeding*, **35**, 1–8.

Henderson, I.R. & Bomblies, K. (2021) Evolution and plasticity of genome-wide meiotic recombination rates. *Annual Review of Genetics*, **55**, 23–43.

Kearsey, M., Ramsay, L., Jennings, D., Lydiate, D., Bohuon, E. & Marshall, D. (1996) Higher recombination frequencies in female compared to male meisoses in *Brassica oleracea*. *Theoretical and Applied Genetics*, **92**, 363–367.

Kelly, A., Sharpe, A., Nixon, J., Lydiate, D. & Evans, E. (1997) Indistinguishable patterns of recombination resulting from male and female meioses in *Brassica napus* (oilseed rape). *Genome*, **40**, 49–56.

Kianian, P., Wang, M., Simons, K., Ghavami, F., He, Y., Dukowic-Schulze, S. *et al.* (2018) High-resolution crossover mapping reveals similarities and differences of male and female recombination in maize. *Nature Communications*, **9**, 1–10.

Koo, D.-H., Hong, C.P., Batley, J., Chung, Y.S., Edwards, D., Bang, J.-W. *et al.* (2011) Rapid divergence of repetitive DNAs in Brassica relatives. *Genomics*, **97**, 173–185.

Koo, D.-H., Plaha, P., Lim, Y.P., Hur, Y. & Bang, J.-W. (2004) A high-resolution karyotype of *Brassica rapa* ssp. *pekinensis* revealed by pachytene analysis and multicolor fluorescence in situ hybridization. *Theoretical and Applied Genetics*, **109**, 1346–1352.

Lashermes, P., Combes, M.-C., Prakash, N., Trouslot, P., Lorieux, M. & Charrier, A. (2001) Genetic linkage map of *Coffea canephora*: effect of segregation distortion and analysis of recombination rate in male and female meioses. *Genome*, **44**, 589–595.

Lawrence, E.J., Gao, H., Tock, A.J., Lambing, C., Blackwell, A.R., Feng, X. *et al.* (2019) Natural variation in TBP-ASSOCIATED FACTOR 4b controls meiotic crossover and germline transcription in Arabidopsis. *Current Biology*, **29**, 2676–2686.e3.

Lenormand, T. (2003) The evolution of sex dimorphism in recombination. *Genetics*, **163**, 811–822.

Lenormand, T. & Dutheil, J. (2005) Recombination difference between sexes: a role for haploid selection. *PLoS Biology*, **3**, e63.

Li, H. & Durbin, R. (2009) Fast and accurate short read alignment with burrows-wheeler transform. *Bioinformatics*, **25**, 1754–1760.

Li, H., Handsaker, B., Wysoker, A., Fennell, T., Ruan, J., Homer, N. *et al.* (2009) The sequence alignment/map format and SAMtools. *Bioinformatics*, **25**, 2078–2079.

Li, X., Li, L. & Yan, J. (2015) Dissecting meiotic recombination based on tetrad analysis by single-microspore sequencing in maize. *Nature Communications*, **6**, 1–9.

Li, Z., Wang, M., Lin, K., Xie, Y., Guo, J., Ye, L. *et al.* (2019) The bread wheat epigenomic map reveals distinct chromatin architectural and evolutionary features of functional genetic elements. *Genome Biology*, **20**, 1–16.

Lian, Q., Solier, V., Walkemeier, B., Durand, S., Huettel, B., Schneeberger, K. *et al.* (2022) The megabase-scale crossover landscape is largely independent of sequence divergence. *Nature Communications*, **13**, 1–11.

Lian, Q., Solier, V., Walkemeier, B., Huettel, B. & Schneeberger, K. (2022) The megabase-scale crossover landscape is independent of sequence divergence. *bioRxiv*. Available from: https://doi.org/10.1101/2022.01.10.474936

Lim, K.-B., De Jong, H., Yang, T.-J., Park, J.-Y., Kwon, S.-J., Kim, J.S. *et al.* (2005) Characterization of rDNAs and tandem repeats in the heterochromatin of *Brassica rapa*. *Molecules and Cells*, **19**, 436–444.

Lim, K.B., Yang, T.J., Hwang, Y.J., Kim, J.S., Park, J.Y., Kwon, S.J. *et al.* (2007) Characterization of the centromere and peri-centromere retrotransposons in *Brassica rapa* and their distribution in related *Brassica* species. *The Plant Journal*, **49**, 173–183.

Luo, C., Li, X., Zhang, Q. & Yan, J. (2019) Single gametophyte sequencing reveals that crossover events differ between sexes in maize. *Nature Communications*, **10**, 1–8.

Marand, A.P., Jansky, S.H., Gage, J.L., Hamernik, A.J., de Leon, N. & Jiang, J. (2019) Residual heterozygosity and epistatic interactions underlie the complex genetic architecture of yield in diploid potato. *Genetics*, **212**, 317–332.

Marand, A.P., Jansky, S.H., Zhao, H., Leisner, C.P., Zhu, X., Zeng, Z. *et al.* (2017) Meiotic crossovers are associated with open chromatin and enriched with stowaway transposons in potato. *Genome Biology*, **18**, 1–16.

Marçais, G., Delcher, A.L., Phillippy, A.M., Coston, R., Salzberg, S.L. & Zimin, A. (2018) MUMmer4: a fast and versatile genome alignment system. *PLoS Computational Biology*, **14**, e1005944.

Martin, O.C. & Wagner, A. (2009) Effects of recombination on complex regulatory circuits. *Genetics*, **183**, 673–684.

McKenna, A., Hanna, M., Banks, E., Sivachenko, A., Cibulskis, K., Kernytsky, A. *et al.* (2010) The genome analysis toolkit: a MapReduce framework for analyzing next-generation DNA sequencing data. *Genome Research*, **20**, 1297–1303.

Melamed-Bessudo, C. & Levy, A.A. (2012) Deficiency in DNA methylation increases meiotic crossover rates in euchromatic but not in heterochromatic regions in Arabidopsis. *Proceedings of the National Academy of Sciences of the United States of America*, **109**, E981–E988.

Melamed-Bessudo, C., Yehuda, E., Stuitje, A.R. & Levy, A.A. (2005) A new seed-based assay for meiotic recombination in *Arabidopsis thaliana*. *The Plant Journal*, **43**, 458–466.

Mercier, R., Mézard, C., Jenczewski, E., Macaisne, N. & Grelon, M. (2015) The molecular biology of meiosis in plants. *Annual Review of Plant Biology*, **66**, 297–327.

Mézard, C., Jahns, M.T. & Grelon, M. (2015) Where to cross? New insights into the location of meiotic crossovers. *Trends in Genetics*, **31**, 393–401.

Mezard, C., Vignard, J., Drouaud, J. & Mercier, R. (2007) The road to crossovers: plants have their say. *Trends in Genetics*, **23**, 91–99.

Mieulet, D., Aubert, G., Bres, C., Klein, A., Droc, G., Vieille, E. *et al.* (2018) Unleashing meiotic crossovers in crops. *Nature Plants*, **4**, 1010–1016.

Mirouze, M., Lieberman-Lazarovich, M., Aversano, R., Bucher, E., Nicolet, J., Reinders, J. *et al.* (2012) Loss of DNA methylation affects the recombination landscape in Arabidopsis. *Proceedings of the National Academy of Sciences of the United States of America*, **109**, 5880–5885.

Modliszewski, J.L. & Copenhaver, G.P. (2017) Meiotic recombination gets stressed out: CO frequency is plastic under pressure. *Current Opinion in Plant Biology*, **36**, 95–102.

Muller, H.J. (1916) The mechanism of crossing-over. IV. *The American Naturalist*, **50**, 421–434.

Nei, M. (1967) Modification of linkage intensity by natural selection. *Genetics*, **57**, 625–641.

Nordborg, M., Hu, T.T., Ishino, Y., Jhaveri, J., Toomajian, C., Zheng, H. *et al.* (2005) The pattern of polymorphism in *Arabidopsis thaliana*. *PLoS Biology*, **3**, e196.

Osman, K., Higgins, J.D., Sanchez-Moran, E., Armstrong, S.J. & Franklin, F.C.H. (2011) Pathways to meiotic recombination in *Arabidopsis thaliana*. *New Phytologist*, **190**, 523–544.

Paape, T., Zhou, P., Branca, A., Briskine, R., Young, N. & Tiffin, P. (2012) Fine-scale population recombination rates, hotspots, and correlates of recombination in the *Medicago truncatula* genome. *Genome Biology and Evolution*, **4**, 726–737.

Pelé, A., Falque, M., Trotoux, G., Eber, F., Negre, S., Gilet, M. *et al.* (2017) Amplifying recombination genome-wide and reshaping crossover landscapes in brassicas. *PLoS Genetics*, **13**, e1006794.

Quinlan, A.R. & Hall, I.M. (2010) BEDTools: a flexible suite of utilities for comparing genomic features. *Bioinformatics*, **26**, 841–842.

Raz, A., Dahan-Meir, T., Melamed-Bessudo, C., Leshkowitz, D. & Levy, A.A. (2021) Redistribution of meiotic crossovers along wheat chromosomes by virus-induced gene silencing. *Frontiers in Plant Science*, **11**, 2332.

Rommel Fuentes, R., Hesselink, T., Nieuwenhuis, R., Bakker, L., Schijlen, E., van Dooijeweert, W. *et al.* (2020) Meiotic recombination profiling of interspecific hybrid F1 tomato pollen by linked read sequencing. *The Plant Journal*, **102**, 480–492.

Rousseau-Gueutin, M., Belser, C., Da Silva, C., Richard, G., Istace, B., Cruaud, C. *et al.* (2020) Long-read assembly of the Brassica napus reference genome Darmor-bzh. *GigaScience*, **9**, giaa137.

Rowan, B.A., Heavens, D., Feuerborn, T.R., Tock, A.J., Henderson, I.R. & Weigel, D. (2019) An ultra high-density *Arabidopsis thaliana* crossover map that refines the influences of structural variation and epigenetic features. *Genetics*, **213**, 771–787.

Sardell, J.M. & Kirkpatrick, M. (2020) Sex differences in the recombination landscape. *The American Naturalist*, **195**, 361–379.

Séguéla-Arnaud, M., Crismani, W., Larchevêque, C., Mazel, J., Froger, N., Choinard, S. *et al.* (2015) Multiple mechanisms limit meiotic crossovers: TOP3α and two BLM homologs antagonize crossovers in parallel to FANCM. *Proceedings of the National Academy of Sciences of the United States of America*, **112**, 4713–4718.

Serra, H., Choi, K., Zhao, X., Blackwell, A.R., Kim, J. & Henderson, I.R. (2018) Interhomolog polymorphism shapes meiotic crossover within the Arabidopsis RAC1 and RPP13 disease resistance genes. *PLoS Genetics*, **14**, e1007843.

Spencer, C.C.A., Deloukas, P., Hunt, S., Mullikin, J., Myers, S., Silverman, B. *et al.* (2006) The influence of recombination on human genetic diversity. *PLoS Genetics*, **2**, e148.

Sturtevant, A.H. (1915) The behavior of the chromosomes as studied through linkage. *Zeitschrift für induktive Abstammungs-und Vererbungslehre*, **13**, 234–287.

Swagatika, S. & Tomar, R. (2016) Modulation of epigenetics by environmental toxic molecules. *Advances in Molecular Toxicology*, **10**, 361–389.

Wijnker, E. & de Jong, H. (2008) Managing meiotic recombination in plant breeding. *Trends in Plant Science*, **13**, 640–646.

Wu, J., Mizuno, H., Hayashi-Tsugane, M., Ito, Y., Chiden, Y., Fujisawa, M. *et al.* (2003) Physical maps and recombination frequency of six rice chromosomes. *The Plant Journal*, **36**, 720–730.

Yelina, N.E., Choi, K., Chelysheva, L., Macaulay, M., De Snoo, B., Wijnker, E. *et al.* (2012) Epigenetic remodeling of meiotic crossover frequency in *Arabidopsis thaliana* DNA methyltransferase mutants. *PLoS Genetics*, **8**, e1002844.

Zhu, L., Fernández-Jiménez, N., Szymanska-Lejman, M., Pelé, A., Underwood, C.J., Serra, H. *et al.* (2021) Natural variation identifies SNI1, the SMC5/6 component, as a modifier of meiotic crossover in Arabidopsis. *Proceedings of the National Academy of Sciences of the United States of America*, **118**, e2021970118.

Ziolkowski, P.A., Berchowitz, L.E., Lambing, C., Yelina, N.E., Zhao, X., Kelly, K.A. *et al.* (2015) Juxtaposition of heterozygous and homozygous regions causes reciprocal crossover remodelling via interference during Arabidopsis meiosis. *eLife*, **4**, e03708.

Ziolkowski, P.A., Underwood, C.J., Lambing, C., Martinez-Garcia, M., Lawrence, E.J., Ziolkowska, L. *et al.* (2017) Natural variation and dosage of the HEI10 meiotic E3 ligase control Arabidopsis crossover recombination. *Genes & Development*, **31**, 306–317.